AGU PUBLICATIONS

Journal of Advances in Modeling Earth Systems

RESEARCH ARTICLE

10.1002/2016MS000683

Inter-model comparison of subseasonal tropical variability in aquaplanet experiments: Effect of a warm pool

Stephanie Leroux[1,2], Gilles Bellon[1,3], Romain Roehrig[1], Mihaela Caian[4], Nicholas P. Klingaman[5], Jean-Philippe Lafore[1], Ionela Musat[6], Catherine Rio[6], and Sophie Tyteca[1]

[1]CNRM UMR 3589, Météo-France/CNRS, Toulouse, France, [2]Laboratoire de Glaciologie et Géophysique de l'Environnement, LGGE UMR 5183, CNRS/Univ. Grenoble Alpes, Grenoble, France, [3]Department of Physics, University of Auckland, Auckland, New Zealand, [4]SMHI, Norrköping, Sweden, [5]National Centre for Atmospheric Science-Climate and Department of Meteorology, University of Reading, Reading, UK, [6]Laboratoire de Météorologie Dynamique/IPSL/UPMC/CNRS

Key Points:
- Subseasonal tropical variability compared in six AGCM aquaplanets with and without a warm pool
- MJO-like variability appears over the warm pool in only half the models
- Tropical-wave characteristics in aquaplanet experiments consistent with those in CMIP and AMIP simulations

Correspondence to:
S. Leroux,
stephanie.leroux@univ-grenoble-alpes.fr

Citation:
Leroux, S., G. Bellon, R. Roehrig, M. Caian, N. P. Klingaman, J.-P. Lafore, I. Musat, C. Rio, and S. Tyteca (2016), Inter-model comparison of subseasonal tropical variability in aquaplanet experiments: Effect of a warm pool, *J. Adv. Model. Earth Syst.*, *8*, 1526–1551, doi:10.1002/2016MS000683.

Received 31 MAR 2016
Accepted 23 AUG 2016
Accepted article online 8 SEP 2016
Published online 7 OCT 2016

Abstract This study compares the simulation of subseasonal tropical variability by a set of six state-of-the-art AGCMs in two experiments in aquaplanet configuration: a zonally symmetric experiment, and an experiment with a warm pool centered on the equator. In all six models, the presence of the warm pool generates zonal asymmetries in the simulated mean states in the form of a "Gill-type" response, made more complex by feedbacks between moisture, convective heating and circulation. Noticeable differences appear from one model to another. Only half the models simulate mean low-level equatorial westerlies over the warm pool area. The presence of the warm pool can also favor the development of large-scale variability consistent with observed Madden-Julian Oscillation (MJO) characteristics, but this happens only in half the models. Our results do not support the idea that the presence of the warm pool and/or of mean low-level equatorial westerlies are sufficient conditions for MJO-like variability to arise in the models. Comparing spectral characteristics of the simulated Convectively Coupled Equatorial Waves (CCEWs) in the aquaplanet experiments and the corresponding coupled atmosphere-ocean (i.e., CMIP) and atmosphere-only (i.e., AMIP) simulations, we also show that there is more consistency for a given model across its configurations, than for a given configuration across the six models. Overall, our results confirm that the simulation of subseasonal variability by given model is significantly influenced by the parameterization of subgrid physical processes (most-likely cloud processes), both directly and through modulation of the mean state.

1. Introduction

1.1. Motivation

Tropical rainfall is organized on a wide range of spatial and temporal scales that remain a challenge to simulate in state-of-the-art general circulation models (GCMs). Observed individual clouds and mesoscale convective systems (MCSs) along the Inter-Tropical Convergence Zone (ITCZ) are often organized into larger zonally propagating features commonly referred to as Convectively Coupled Equatorial Waves (CCEWs) [e.g., *Kiladis et al.*, 2009]. These features - such as Equatorial Kelvin waves, Equatorial Rossby waves and Mixed Rossby-Gravity waves - can in turn be modulated by the planetary-scale eastward propagating Madden-Julian Oscillation (MJO) [*Madden and Julian*, 1972; *Zhang*, 2005]. The latter represents a major source of predictability on intraseasonal scales in the tropics [e.g., *Waliser et al.*, 2003; *Gottschalck et al.*, 2010], and its influence extends to the midlatitudes [*Cassou*, 2008; *Moore et al.*, 2010]. The observed CCEWs show consistency with the classical shallow-water equatorial-wave theory proposed by *Matsuno* [1966], but no comprehensive theory has yet emerged to explain all aspects of the intraseasonal MJO [e.g., *Zhang et al.*, 2013].

GCMs show a large variety of behaviors in the way they simulate subseasonal tropical variability. None of them can reproduce satisfyingly the entire observed space-time spectrum, even if noticeable improvements are overall achieved from one generation of GCMs to the next (e.g., from CMIP3 to CMIP5 in *Hung et al.* [2013]). Improving how the MJO is simulated undoubtedly remains an important challenge for any GCM in the tropics [e.g., *Zhang et al.*, 2013; *Hung et al.*, 2013; *Jiang et al.*, 2015]. It is seen that the different characteristics of the MJO are reproduced with various degrees of success by each GCM. For example, some models produce an oscillation on intraseasonal scales but with only weak propagation. Others can simulate a

propagating mode but significant differences are still seen in the vertical structure between models [*Jiang et al*., 2015; *Klingaman et al*., 2015; *Xavier et al*., 2015]. From inter-GCM comparison studies such as *Hung et al*. [2013], it also appears that there is no best nor worst model for the entire spectrum of variability. For instance, the ability to simulate an MJO-like oscillation does not seem necessarily correlated with the degree of success to which the same model simulates the different CCEWs. This variety of behavior among GCMs reflects the strong dependence of the tropical variability on how subgrid physical processes (phase changes, turbulence, radiation) are parameterized. Schemes for convective triggering, cloud types, or surface fluxes are thought to play a significant role in the mechanisms at play in CCEWs and the MJO [e.g., *Jiang et al*., 2015; *Klingaman et al*., 2015; *Sobel and Maloney*, 2012; *Kiladis et al*., 2009]. Those parameterizations are also likely to act on the model's mean state, which in turn is thought to modulate the simulated tropical variability [e.g., *Han and Khouider*, 2010; *Inness et al*., 2003].

Understanding the mechanisms of intraseasonal variability and the causes for differences in GCM behavior is complicated by various factors. The characteristics of the intraseasonal oscillation vary with the seasonal cycle: the "canonical" MJO is more often observed in boreal winter, while in summer the oscillation has a more pronounced northward propagation and interacts with the Asian monsoon [*Wang et al*., 2006; *Zhang*, 2005]. How distinct are the mechanisms at play in both seasons remains an open question. Coupling with an interactive ocean is also seen to amplify or improve to differing degrees the simulation of the MJO in different GCMs, and both surface fluxes and changes in the mean state seem to be involved [e.g., *DeMott et al*., 2014; *Jiang et al*., 2015]. Interactions with heterogeneous land-sea surface and orography might also interfere in how the MJO propagates over the Maritime continent [e.g., *Peatman et al*., 2014].

In this paper we present an inter-model comparison study documenting the variety of behavior among state-of-the-art GCMs in the way they simulate tropical subseasonal variability, and how the choices made for the parameterizations of the subgrid scale physical processes might impact on this subseasonal variability.

Our approach follows the idea previously promoted by *Hoskins et al*. [1999], *Neale and Hoskins* [2000], *Blackburn and Hoskins* [2013] that aquaplanet experiments provide a useful benchmark to compare Atmospheric-GCMs (AGCMs) with simplified boundary conditions and forcing––namely a water-covered Earth to which is applied an idealized time-independent sea surface temperature (SST), and fixed equinoctial radiative forcing. The use of the simplified aquaplanet forcing and boundary conditions rules out some of the influencing factors listed previously, such as the role of the land-sea contrasts, orography, ocean coupling, or seasonal changes in the mean state. By design, the focus is thus on differences in model behaviors due to differences in dynamical core, spatial resolution, and subgrid parameterizations. Using this idealized set-up to study the tropical climate and its subseasonal variability builds on a diversed body of earlier work with aquaplanets. Some aspects are reviewed in the next section, followed by an outline of the paper.

1.2. Earlier Work With Aquaplanets

1.2.1. Sensitivity to the Imposed SST Boundary Condition

A primary objective of earlier aquaplanet studies has been to investigate the sensitivity of full-physics AGCMs mean states to various zonally symmetric SST boundary conditions. *Hess et al*. [1993] pointed out for the first time the large sensitivity of the simulated mean state to both the meridional gradient in SST and the model's parameterizations. More recently, the inter-model comparison project APE (Aqua-Planet Experiment) extended the approach to compare 16 aquaplanet AGCMs and several idealized SST boundary conditions symmetric about the equator [see *Williamson et al*., 2013, and other APE references therein]. The zonal-mean circulation was shown to depend on the imposed SST gradient: as the SST latitudinal distribution flattens in the tropics, the Hadley circulation weakens and shifts poleward, and the midlatitude jet cores move poleward. The extent of these variations is however model-dependent. Besides, the stationary regime of the tropical precipitation is either a single maximum along the equator, or alternatively a double maximum straddling the equator, depending on the imposed meridional SST gradient. A sharply peaked SST profile usually leads to a single-maximum regime, while a flatter SST profile leads to a double-maximum regime. Again, the actual degree of how "peaked" or "flat" it needs to be to switch from one precipitation regime to the other is model-dependent. *Oueslati and Bellon* [2013a] showed that the transition between the single and double maximum regimes in two contrasting aquaplanet models was driven by changes in the low-level convergence forced by the SST gradient, but modulated by dry and moist model-dependent feedbacks.

1.2.2. Tropical Subseasonal Variability (CCEWs and MJO)

A brief overview of the tropical subseasonal variability simulated by the APE models in their control axisymmetric aquaplanet experiment (i.e., forced by a zonally uniform SST pattern) is found in *Williamson et al*. [2013]. Space-time spectral analysis of the tropical precipitation showed no clear MJO-like variability in any of the models. Despite the unified aquaplanet configuration, the CCEWs simulated by these models exhibited a large diversity. The inter-model differences appeared the largest in the vertical structure of the synoptic waves and especially when looking at the convective and stratiform heating [*Nakajima et al*., 2013a]. Significant differences were also found in the phase relationship between precipitation and low-level convergence in the waves. Overall the APE results confirmed the difficulties of the AGCMs in coupling the moisture and the flow anomalies, underlying the essential role of the parameterization schemes in the simulated variability.

MJO-like tropical variability in aquaplanets has also been the specific focus of a number of studies since the pioneer papers. For example, *Hayashi and Sumi* [1986] and *Swinbank et al*. [1988] described a "30 day oscillation" propagating eastward around the tropics with the structure of a large Kelvin wave, of which the propagation speed and periodicity seemed sensitive to moisture effects. More recently, *Kang et al*. [2013] showed that the properties (horizontal scale and structure, speed and periodicity) of the Kelvin waves simulated in a zonally symmetric aquaplanet experiment were dependent on the meridional SST gradient. For a flatter SST latitudinal distribution at the equator, the low-level wind Kelvin wave signal appeared to slow down and to couple with a westward equatorial Rossby wave. The authors suggested that the resulting "coupled Kelvin-Rossby wavepacket" might provide some insight in the mechanisms of the observed MJO.

A growing number of studies alternatively discuss the observed MJO as a "moisture mode" of which the destabilization and eastward propagation can be analyzed through the terms of its budget of Moist Static Energy (MSE) [see *Sobel and Maloney*, 2012, and references therein]. In this framework, *Maloney et al*. [2010] performed sensitivity experiments with an aquaplanet model to investigate the conditions under which such an eastward intraseasonal moisture mode appeared, and analyzed the sources and sinks of its MSE budget. Their SST boundary condition was derived from averaging and smoothing the observed Indian-Pacific SST. The geographical distribution was asymmetric in longitude and latitude and included a wavenumber 1 warm pool peaking at 30° C, centered just south of the equator, and with reduced meridional SST gradient to one third of observed gradient. Their study showed that the presence of this warm pool, and the low-level mean westerly flow it induced locally on the equator, was a necessary condition, in their model, for the MJO-like moisture mode to arise. This moisture mode did not arise in the control experiment where the zonally asymmetric SST pattern was replaced by its corresponding zonal average. The MSE budget of their MJO-like moisture mode highlighted that (1) the mode was destabilized by wind-induced latent heat flux anomalies at the surface, and (2) its eastward propagation resulted from the zonal advection of humidity (both through the mean zonal and eddy transport). In addition, the destabilizing role of the cloud radiative feedbacks was also also pointed out in a companion paper by *Landu and Maloney* [2011]. However, *Maloney et al*. [2010] noted that the processes contributing to the eastward propagation of the mode in their aquaplanet (*zonal* advection of humidity) were not consistent with those in their standard GCM experiment [*Maloney*, 2009], where *meridional* humidity advection was the dominant term. More specifically, they had observed in their standard GCM experiment a relative humidification ahead of the moisture mode subsequent to the inhibition of the eddies' drying effect by the large-scale flow (as eddies mix the drier air from the subtropics with the wetter air from the equator). This inconsistency between the aquaplanet experiment and its standard GCM counterpart points out some limits in the use of aquaplanets to interpret AGCM behaviors in more realistic configurations. It also remains unclear how model-dependent those results are. It is for example noted that the relative contribution of the latent heat fluxes to the MSE budget of the MJO is too large in the model in *Maloney* [2009] and *Maloney et al*. [2010], compared to radiative fluxes, unlike observed. This was ascribed later on to radiative feedbacks being too weak in that same model [*Hannah and Maloney*, 2011, 2014]. In other words, one model might produce an MJO mode for "wrong" reasons compensating for other aspects of the moist physics that would be unrealistically simulated. This possibility strongly argues in favor of carrying out inter-model comparison work in addition to this type of in-depth processes studies focused on a single model.

The warm pool seen as a necessary condition for the MJO was for example questioned by *Andersen and Kuang* [2012] who obtained an MJO-like mode in an aquaplanet experiment for which a zonally symmetric

SST is applied. The configuration of their model is however relatively far from the one of *Maloney et al.* [2010] as they ran an aquaplanet with a super-parametrized convection (SPCAM), seasonally varying insolation and a zonally symmetric SST peaking at 5° N. In their case, the MSE budget of their MJO-like mode suggested that the radiative feedbacks were the main source of MSE in phase with the precipitation (destabilizing role) rather than latent heat fluxes. The main source of MSE ahead of the precipitation envelope was also found to be the meridional advection rather than the zonal advection as in *Maloney et al.* [2010]'s aquaplanet.

1.3. Outline

The present study was carried out as part the EMBRACE (Earth system Model Bias Reduction and assessing Abrupt Climate change) project, funded by the European Union's 7th Framework Program. EMBRACE provided the framework and opportunity to gather a set of six up-to-date AGCMs and to perform specifically designed aquaplanet experiments with them. Building on the existing literature presented above, we take here the point of view of an inter-model and inter-configuration comparison, in order to investigate the following aspects: How do these GCMs in aquaplanet configuration compare in the way they simulate subseasonal tropical variability? To what extent the variety of behaviors known to exist among the full "CMIP-type" models remains in an idealized aquaplanet setting? How sensitive are the aquaplanet GCMs to breaking the longitudinal symmetry of the SST boundary conditions with an idealized "warm pool"? In particular, is this a necessary condition for MJO-like intraseasonal variability to appear? The focus here is on documenting whether consistent results and behaviors are seen among the models rather than describing in full details the behavior of each of the six aquaplanet models individually. We further extend the inter-model comparison across configurations by comparing spectral characteristics of the simulated subseasonal variability in the aquaplanet experiments and in the corresponding coupled atmosphere-ocean (i.e., CMIP) and atmosphere-only (i.e., AMIP), in order to investigate how consistent are these three configurations for each GCM.

Section 2 presents the six AGCMs involved in the inter-comparison, and gives the details of the numerical set-up for the aquaplanet experiments. Sections 3 and 4 respectively compare the tropical mean state and subseasonal variability simulated by this set of models. Section 5 then discusses possible links between mean state and subseasonal variability in the context of existing literature. A summary and some concluding remarks are finally given in section 6.

2. Aquaplanet Set-up and Models

2.1. Zonally Symmetric Reference SST (QOBS)

We choose to use as our reference SST boundary condition the zonally symmetric SST (labeled "QOBS" in the following), that was previously designed in the literature to resemble the mean observed SST in the Indo-Pacific region [e.g., *Neale and Hoskins*, 2000]. The QOBS latitudinal SST profile is defined as:

$$SST_{Qobs} = 0.5\left[27\left(1-\sin^2\left(\frac{\pi\times \mathrm{lat}}{120}\right)\right)\right] + 0.5\left[27\left(1-\sin^4\left(\frac{\pi\times \mathrm{lat}}{120}\right)\right)\right]$$

where lat (the latitude in degrees) is between $[-60^o, 60^o]$, and $SST_{Qobs}=0$ otherwise.

This is the same idealized SST as used for the zonally symmetric aquaplanet experiments of the CMIP5 protocol [*Taylor et al.*, 2012]. It differs from the control SST in the APE project, the latter having a more sharply peaked latitudinal distribution about the equator. The APE control SST was shown to induce strong midlatitude jets, located closer to the equator than observed. It was also shown to yield faster westerlies than observed in the equatorial upper levels, that were suspected to influence in turn the characteristics of the tropical variability [*Nakajima et al.*, 2013a, 2013b].

2.2. Adding an Idealized Warm Pool (QOBS+WP)

In addition to the reference zonally symmetric experiment, we also perform an experiment (labeled QOBS+WP in the following) in which a warm-pool-like temperature anomaly is added to SST_{Qobs}. The warm

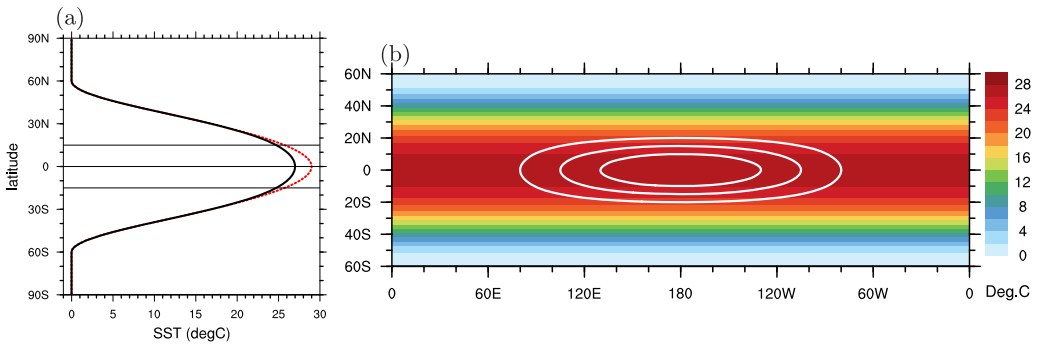

Figure 1. (a) Meridional SST section along longitude 180° in the zonally symmetric experiment (QOBS, solid black) and in the experiment with a warm-pool (QOBS+WP, dotted red). (b) SST (° C) in the QOBS experiment (shading), and SST anomaly (QOBS+WP minus QOBS) contoured in solid white every 0.5° C (zero omitted).

pool is centered on the equator, at longitude $\mathrm{lon}_0 = 180^o$, with a half-length of $\Lambda_{lat} = 30^o$ in latitude and $\Lambda_{\mathrm{lon}} = 150^o$ in longitude. The SST anomaly is $\Delta_{\mathrm{wp}} = +2^o\mathrm{C}$ at the centre of the warm pool.

If $lat \in [-\Lambda_{lat}, +\Lambda_{lat}]$ and $\mathrm{lon} \in [\mathrm{lon}_0 - \Lambda_{\mathrm{lon}}, \mathrm{lon}_0 + \Lambda_{\mathrm{lon}}]$,the SST with warm pool is defined as:

$$SST_{\mathrm{wp}} = SST_{Q\mathrm{obs}} + \Delta_{\mathrm{wp}} \times \cos^2\left(\frac{\pi}{2}\frac{\mathrm{lat}}{\Lambda_{\mathrm{lat}}}\right) \times \cos^2\left(\frac{\pi}{2}\frac{\mathrm{lon} - \mathrm{lon}_0}{\Lambda_{\mathrm{lon}}}\right)$$

where lat and lon are the latitude and longitude in degrees, respectively. Away from the warm pool, $SST_{\mathrm{wp}} = SST_{Q\mathrm{obs}}$. As a summary, the idealized SST boundary conditions used in the QOBS and QOBS+WP experiments are plotted in Figure 1.

The $\Delta_{\mathrm{wp}} = +2^o\mathrm{C}$ maximum anomaly in the warm pool is in the range of the APE protocol, which proposed two warm pool anomalies of $+1^o\mathrm{C}$ and $+3^o\mathrm{C}$. It is also of same order of magnitude as the SST used by *Maloney et al.* [2010] (see their Figure 1) derived from observed time-mean SST in the Indo-Pacific region.

An additional experiment was performed with the six models to test the sensitivity to the size of the warm pool in longitude, with a warm pool of intermediate longitude extension ($\Lambda_{\mathrm{lon}} = 50^o$). Results from this experiment will not be shown for the sake of brevity, but they will be discussed in section 4.4. A few more sensitivity experiments were also performed with one of the models (CNRM-5) to test further the sensitivity of the results to some other aspects of the experimental design. The effect of a more elongated warm pool (half-length $\Lambda_{\mathrm{lon}} = 180^o$) was tested. Another experiment was also performed in the zonally symmetric configuration with a peak SST value on the Equator at 29° C (instead of 27° C in QOBS). Theses sensitivity experiments are also discussed in section 4.4.

2.3. Participating Models

We consider and compare here six AGCMs, run in the aquaplanet set-up described above: CNRM-5, CNRM-PRE6, EC-Earth, MetUM-GA3, IPSL-A, IPSL-B. Their reference papers are listed in Table 1 along with their spatial resolution and information about their convective schemes. None of these GCMs did participate to the earlier APE inter-comparison. Also, APE had involved an older generation of models (contributing to CMIP3) while the models examined in the present paper took part in CMIP5. Two institutes have provided the aquaplanet experiments with two versions of their model: IPSL-A, IPSL-B and CNRM-5, CNRM-PRE6 respectively. In each pair, the two versions differ at least by the set of parameterizations of the subgrid physical processes (deep and shallow convection, boundary-layer turbulence, etc). Both IPSL-A and IPSL-B took part in CMIP5, IPSL-B being at the time the most-recent version of the parameterization set for this model, and IPSL-A being the previous version, run for comparison [*Dufresne et al.*, 2013; *Hourdin et al.*, 2013]. CNRM-5 took part in CMIP5, while CNRM-PRE6 is a preliminary version of the CNRM model being developed for the coming CMIP6. It differs from CNRM-5 by an updated dynamical core, an increased vertical resolution and an entirely new package of parameterizations for subgrid scale moist processes (shallow and deep

Table 1. Participating Models and References

	Model Name	Research Group	Horizontal Res. and Vertical Levels	Model Reference	Convective Scheme Reference
1	CNRM-5	*CNRS Météo-France*	T127 x L31	*Voldoire et al.* [2013]	*Bougeault* [1985] Moisture convergence
2	CNRM-PRE6	*CNRS Météo-France*	T127 x L91	Model in development for CMIP6 (cf. section 2.3)	*Piriou et al.* [2007]; *Guérémy* [2011] CAPE
3	EC-Earth	*Rossby Centre, Swedish Meteo. and Hydro. Institute*	T159 x L42	*Hazeleger et al.* [2012]	*Tiedtke* [1989] CAPE/moisture convergence
4	MetUM-GA3	*Met Office*	N96 x L85	*Walters et al.* [2011]	*Gregory and Rowntree* [1990] CAPE
5	IPSL-A	*IPSL, France*	T63 x L39	*Hourdin et al.* [2006]	*Emanuel* [1991] CAPE/CIN
6	IPSL-B	*IPSL, France*	T63 x L39	*Hourdin et al.* [2013]	*Rio et al.* [2010] *Grandpeix and Lafore* [2010] Available Lifting Energy/Power

convection, boundary layer turbulence and microphysics). A preliminary description of this new package can be found in *Couvreux et al.* [2015] and *Michou et al.* [2015].

Each aquaplanet experiment was run with a constant equinoctial solar forcing for at least 4 years. This 4 year period represents more than ∼32 times the longest period of the variability we aim to diagnose here (i.e., MJO; period T ∼ 45 days). It was also verified that the characteristics of subseasonal variability in the models were established in the first few months and then remained similar from year to year over the entire simulations. The analyses and diagnostics shown in this study are all performed on the daily averaged outputs.

3. Simulated Mean States

The choices made for the parameterizations of the subgrid processes in each model might influence the simulated tropical variability in two ways: (1) via a direct influence on the destabilization and growth processes of the tropical modes [e.g., *Sobel and Maloney*, 2012], or (2) via an indirect influence through a control of the mean state (both dynamics and moisture), which in turn, might influence the way the tropical modes develop (e.g., vertical shear as discussed in *Dias and Kiladis*, [2014] and *Han and Khouider* [2010]). In this section, we therefore present some elements of comparison about the simulated tropical mean states, before the tropical subseasonal variability is shown in section 4.

3.1. Zonally Symmetric Experiment (QOBS)

A significant diversity remains among the six simulated mean states despite the idealized configuration and identical zonally symmetric SST boundary condition, as was suggested by previous studies [e.g., *Williamson et al.*, 2013; *Stevens et al.*, 2013]. This is illustrated in Figure 2 with the zonally averaged 850 hPa zonal and meridional winds, 850 hPa wind convergence and precipitation. Diversity appears in the amplitude of the low-level tropical easterlies, as well as in their location in latitude on both sides of the equator (Figure 2a). Note however that the same model, CNRM-5, stands out as the outlier in all these panels, while the five other models appear more alike regarding the location of the wind gradients and convergence.

The models also differ by the degree to which the trade-winds converge equatorward (Figures 2b and 2c) and by the amplitude and meridional width of the ITCZ precipitation pattern (Figure 2d). The latter is either single- or double- peaked, consistent with the sensitivity to the meridional distribution of SST studied in *Oueslati and Bellon* [2013a]. Recall however that the same SST distribution is applied here to all the models. Thus for this given meridional distribution of SST, the differences between the simulated ITCZs can only be accounted for by the differences in the models' formulations. Note that the two models showing the most pronounced double-peaked precipitation pattern (CNRM-5 and IPSL-A) correspond to the two old versions of the pairs of models provided by CNRM and IPSL. This unrealistic "double-ITCZ" feature, also discussed in *Oueslati and Bellon* [2013b], is not seen anymore in the more recent versions (CNRM-PRE6 and IPSL-B). CNRM-5 was also shown to be the outlier model in term of low-level wind convergence (Figure 2a), which is precisely thought to be the main driver of the ITCZ geometry [*Oueslati and Bellon*, 2013a].

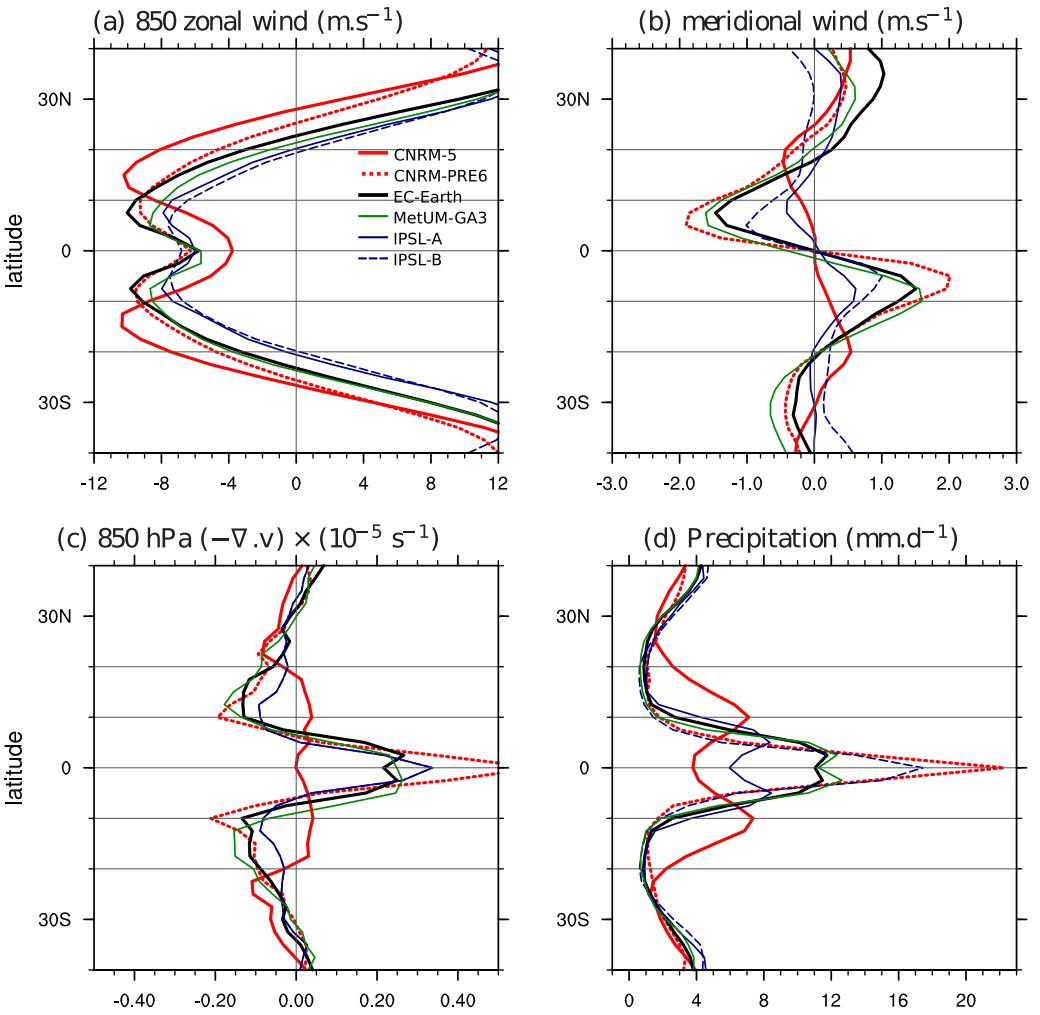

Figure 2. Time-mean zonally averaged (a) zonal and (b) meridional wind components at 850 hPa, (c) horizontal wind convergence at 850 hPa, and (d) precipitation, in the QOBS experiment from the 6 model: thick solid red for CNRM-5, thick dashed red for CNRM-PRE6, thin solid blue for IPSL-A, thin dashed blue for IPSL-B, thick solid black for EC-Earth, and thin solid green for MetUM-GA3.

3.2. Warm-Pool Experiment (QOBS+WP)

The consequences on the mean state of adding a warm pool (experiment QOBS+WP) are shown in Figures 3 and 4 for precipitation and 850 hPa wind. Figure 3 also gives in contours the difference in precipitation relative to the zonally symmetric experiment (QOBS), and Figure 5 gives the difference in 200-to-850 wind shear, and geopotential height at 200 hPa. Adding the warm pool breaks the zonal symmetry of the ITCZ in all the models, with a concentration of precipitation in the warm-pool area, and less precipitation away from the warm pool compared to the QOBS experiment. The two models that had a double ITCZ in QOBS (i.e., CNRM-5 and IPSL-A) now show a single equator-centered peak of precipitation in the warm pool, with only a faint double ITCZ remaining away of the warm-pool region. The degree to which precipitation decreases away from the warm pool is however model dependent. See for example the contrasting precipitation difference QOBS+WP- QOBS in the two models that show a narrow ITCZ in the zonally symmetric case (i.e., CNRM-PRE6 and IPSL-B). The presence of the warm pool also induces modifications in the amplitude of the precipitation pattern within the ITCZ but it is worth noting that the latitudinal extent of the ITCZ itself remains relatively unchanged in the experiments with and without warm pool for a given model. For example, the zonally symmetric ITCZ is very narrow in QOBS for models IPSL-B and CNRM-PRE6 (the 2–4 mm/d contour being contained between 5° S and 5° N), and it remains of similar width in QOBS+WP, even if the SST warm-pool anomaly extends from 20° S to 20° N.

Within the ITCZ, the amplitude of the precipitation change in QOBS+WP relative to QOBS depends on the model, and so is the longitudinal position of the precipitation peak. The latter is seen just east of the center

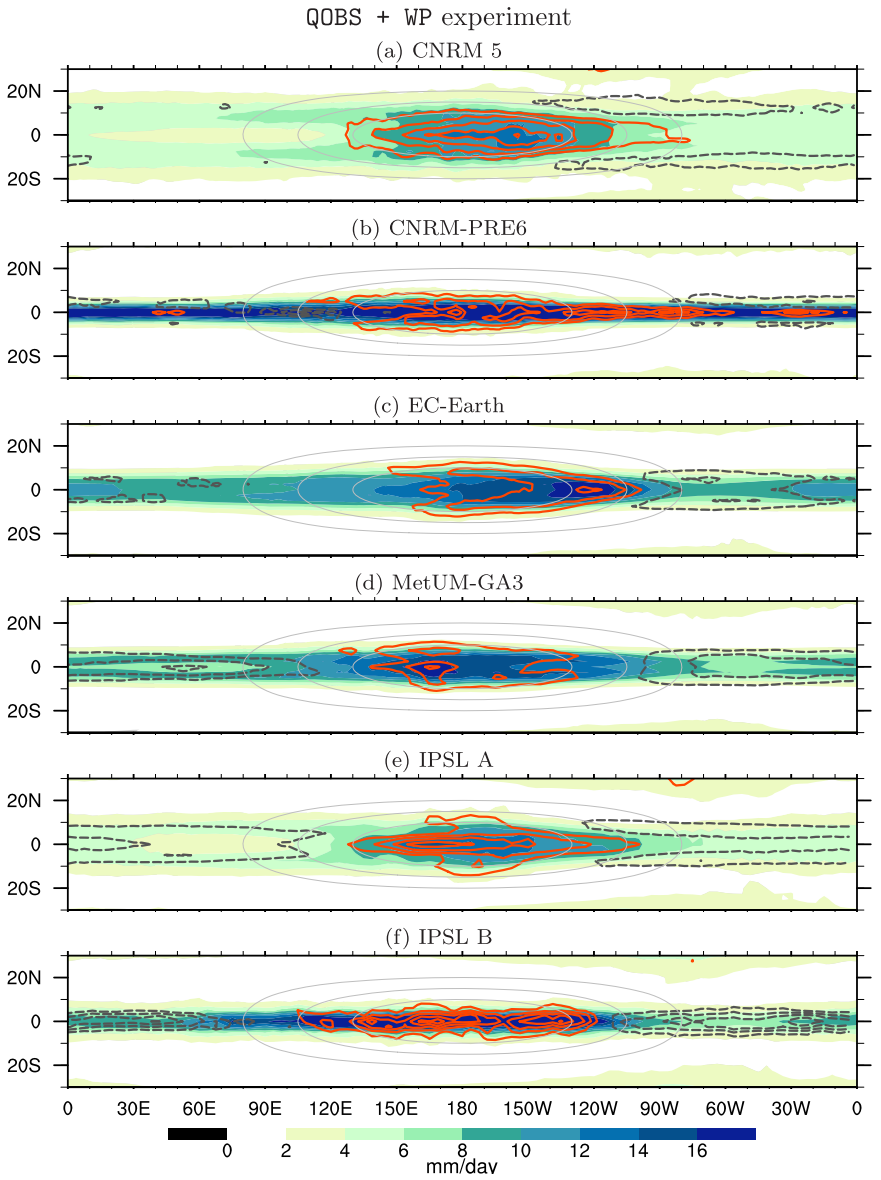

Figure 3. Time-mean precipitation in the QOBS+WP experiment: total field (shading in mm d^{-1}) and anomaly to the zonally symmetric experiment QOBS from the 6 models (contours every 2 mm d^{-1}, zero omitted, solid red for positive values, dashed dark grey for negative values). The SST anomaly in the warm-pool is contoured in light every 0.5°C (zero omitted).

of the warm pool for half of the models (CNRM-5, CNRM-PRE6, EC-Earth) while it appears slightly west of it for the other half (MetUM-GA3, IPSL-A, IPSL-B).

The presence of the warm pool also has the effect of breaking the zonal symmetry of the circulation, as seen from the time-mean 850 hPa wind and 200-to-850 hPa zonal shear in Figures 4 and 5. In the lower levels, the warm pool induces a reinforcement of the equatorward component of the wind on both flanks of the warm pool (i.e., ∼10-15° N and S). The low-level equatorial easterlies strengthen just east of the warm-pool, while they weaken in the western part of the warm pool. In three of the models (CNRM-5, IPSL-A, and EC-Earth), the weakening of the easterlies is such that actual equatorial westerlies appear, consistent with the observed low-level wind mean state in the Indian ocean. We thus find here that only half the models of our set reproduce the behavior seen in *Maloney et al.* [2010] from their single-model aquaplanet study with a warm pool. The presence or absence of these low-level westerlies is consistent in each model from level 850 hPa to the surface (not shown).

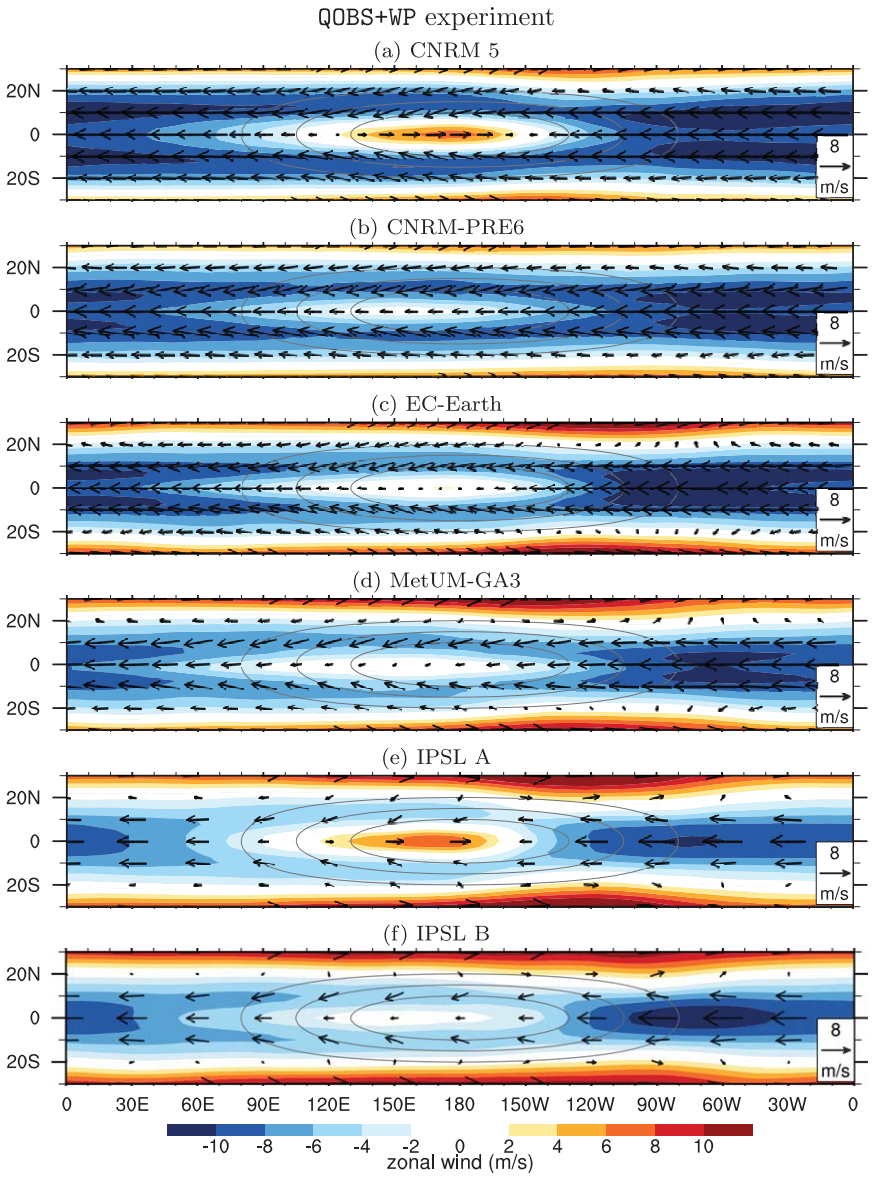

Figure 4. Time-mean horizontal wind at 850 hPa (vectors, see scale on the map), and zonal component (shading, in m s^{-1}) in the QOBS+WP experiment from the 6 models. The SST anomaly in the warm-pool is contoured in light every 0.5°C (zero omitted).

The latitudinal extent of the circulation pattern induced by the warm pool is fairly similar in the six models. The diversity between models is mainly seen in the strength of the circulation change, and in the presence or absence of the low-level westerlies on the equator. The presence of those westerlies is interestingly the main noticeable difference between the two versions of the model pairs (old versus new) provided by CNRM and IPSL: the westerlies arise in the older versions (i.e., CNRM-5 and IPSL-A), which are also the two models with the broader ITCZ band (doubled-peaked in QOBS).

The zonal vertical shear between 200 and 850 hPa decreases above the warm pool and amplify on the equator, away from the warm pool. The three models that simulate low-level westerlies in the warm pool also show the stronger reduction in the vertical shear.

From a more general point of view, Figures 3–5 thus illustrate how a "Gill-type" response of the tropical atmosphere to some localized diabatic heating [*Gill*, 1980] becomes more complex when the full feedbacks between the convective heating and the circulation are modeled. The warmer SST in our warm-pool experiment induces locally an increase of moist convection in the ITCZ that generates a dynamical response of

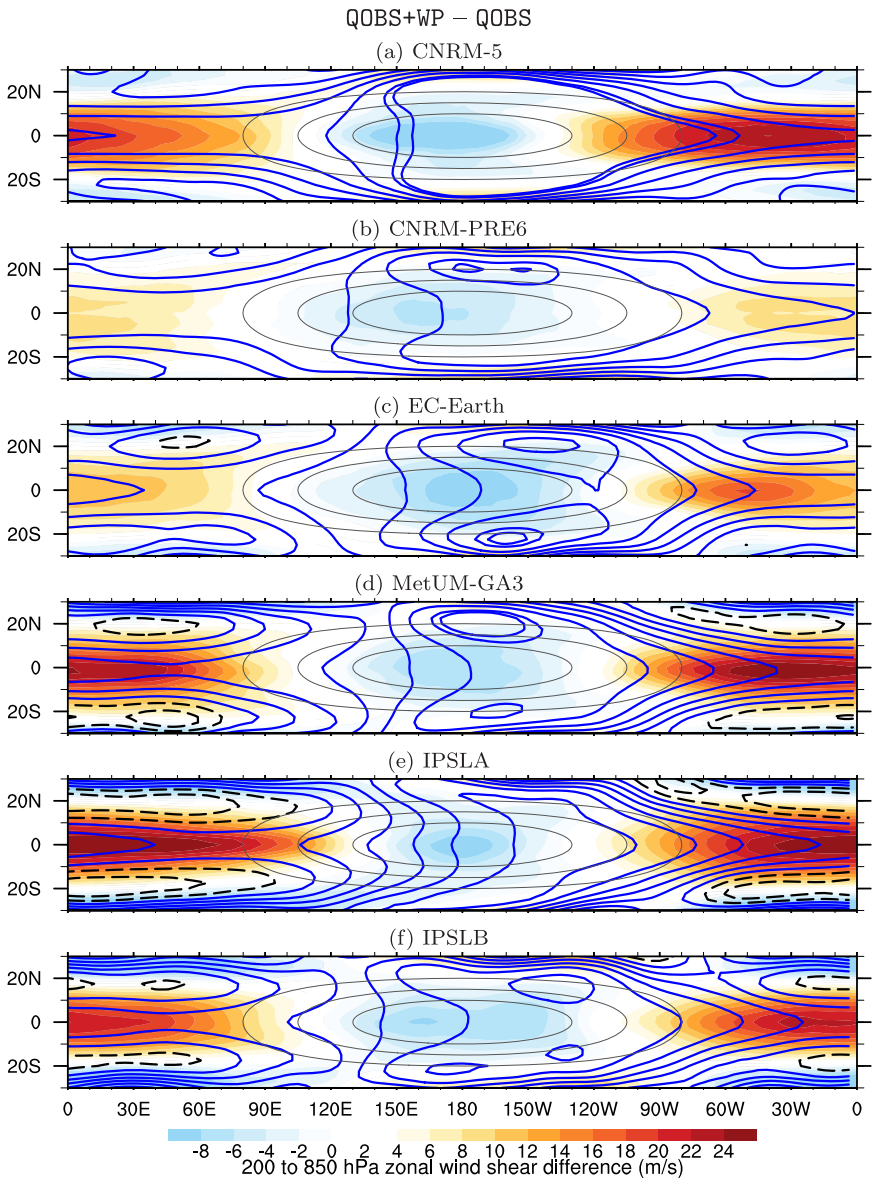

Figure 5. Time-mean difference between QOBS+WP and QOBS experiments of: 200-to-850 hPa zonal wind shear (shading), and of geopotential height (contoured every 15 m, positive values in solid blue, negative values in dashed black). The SST anomaly in the warm-pool is contoured in light every 0.5°C (zero omitted).

the atmosphere (e.g., illustrated with the geopotential height difference in Figure 5), with ascent over the warm pool, as in the Gill symmetric case. However, here the diabatic heating is not imposed but interactive, in that it is influenced in turn by the moist feedbacks from the circulation on the convection. Those feedbacks result in large part from the transport of moisture into the warm-pool region by the dynamical response. These feedbacks generally enhance convection over the warm pool, but they also modulate its spatial distribution. Experiment QOBS+WP thus points out the large sensitivity of the time-mean precipitation and wind response patterns to the models' physics, and thus suggests that such aquaplanet set-ups can be useful to understand this sensitivity better.

In the next section, we examine how tropical subseasonal variability is simulated in these aquaplanet experiments. Given the substantial diversity between the models mean states, it is already clear that both the direct influence of the parameterization choices on the tropical variability, and their indirect influence via changes in the mean state likely remain at play in our idealized aquaplanet set-up.

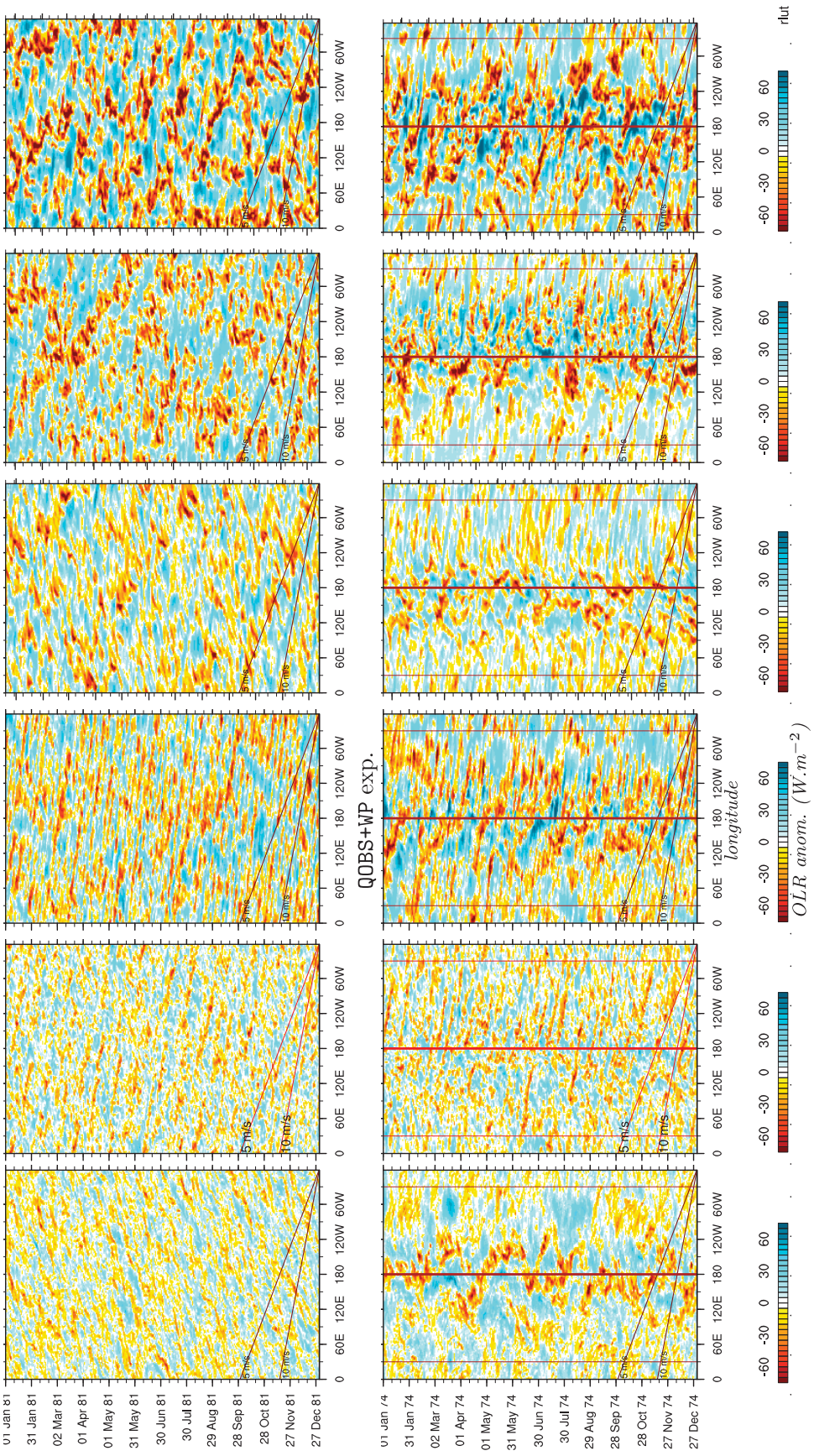

Figure 6. Time-longitude diagrams (hovmoellers) of the OLR anomaly (i.e., after removing the time-mean), averaged between 10° S and 10° N for 1 illustrative year in (left) the QOBS and (right) QOBS+WP experiments from the 6 models.

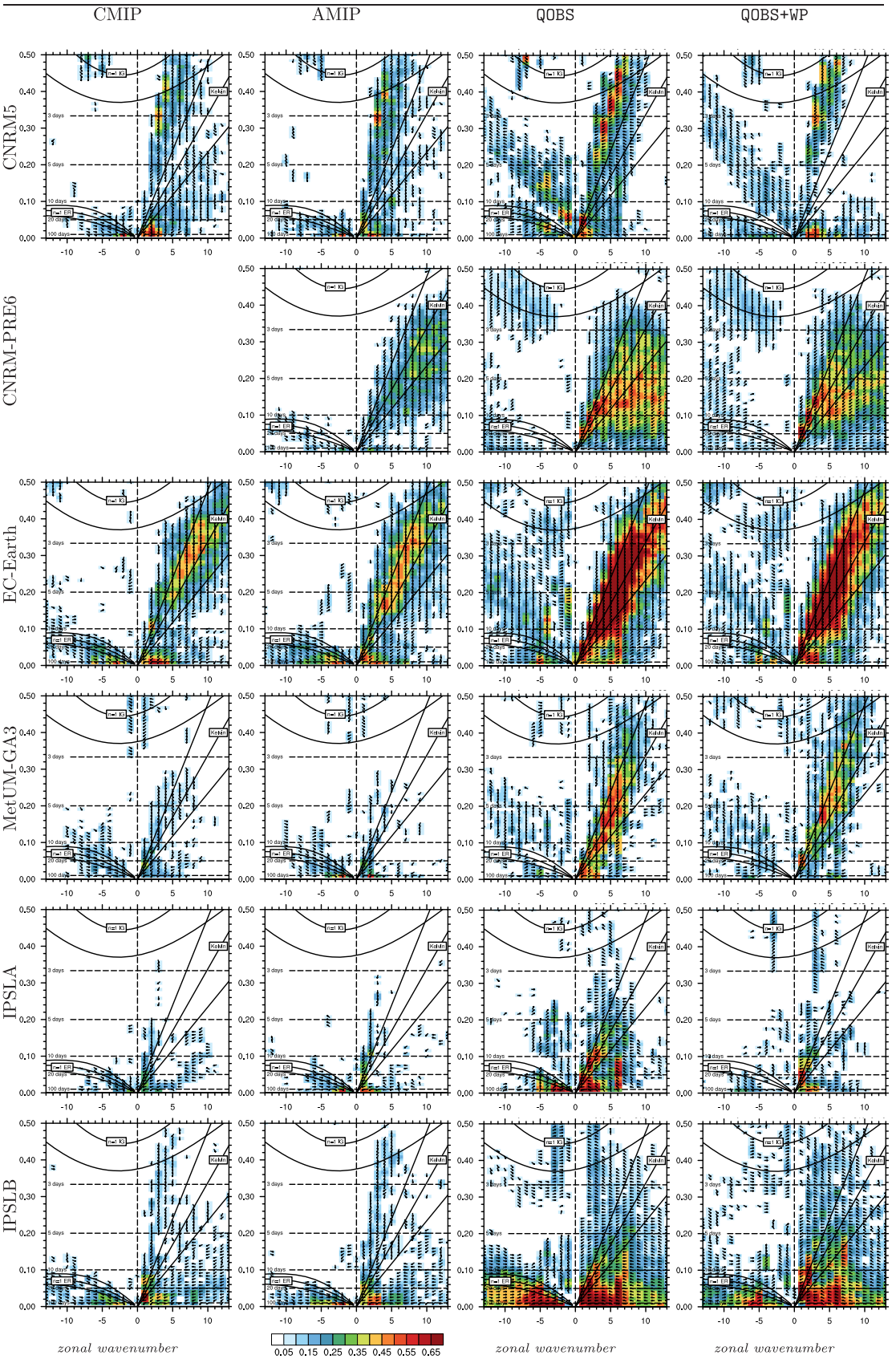

Figure 7. Symmetric component of space-time coherence squared spectra (OLR and U 850 hPa). See text (section 4.1).

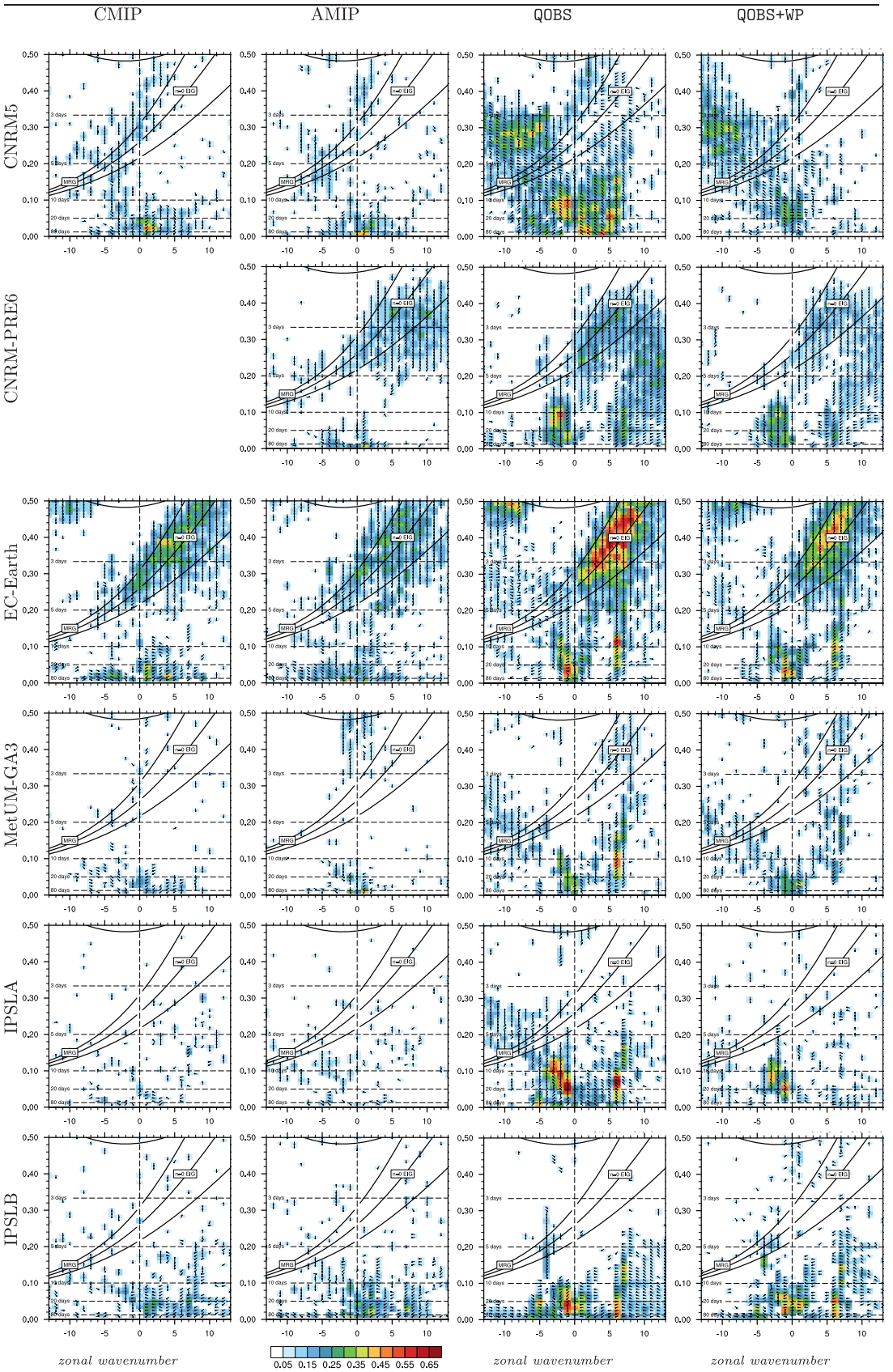

Figure 8. Antisymmetric component of space-time coherence squared spectra (OLR and U 850 hPa). See text (section 4.1).

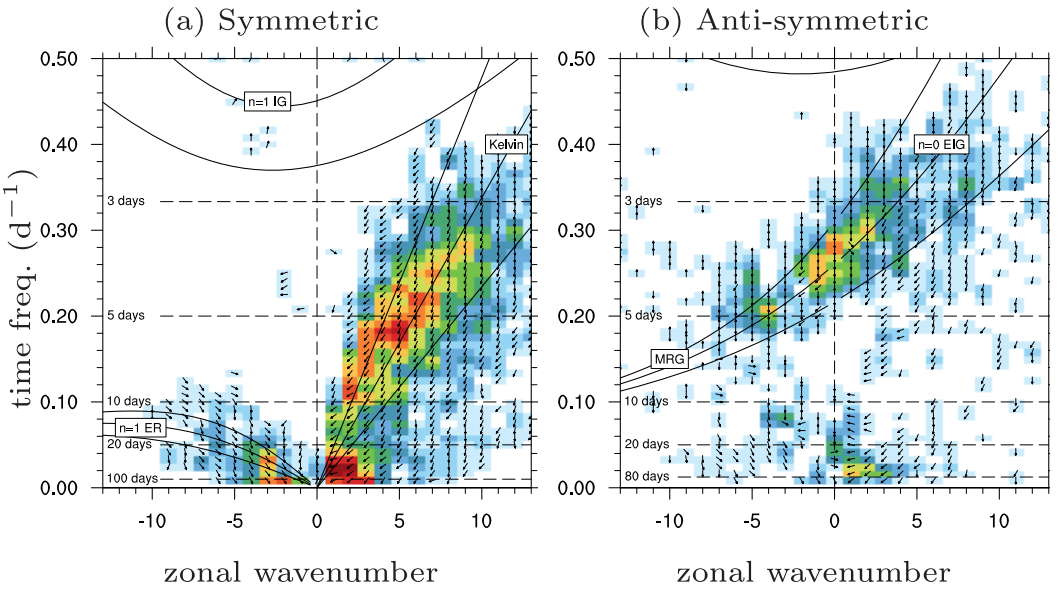

Figure 9. (a) Symmetric and (b) anti-symmetric component of space-time coherence squared spectrum of NOAA OLR and ERA-interim 850 hPa zonal wind. The spectrum is computed on overlapping 120 day time-segments over 2000–2003. Dispersion curves derived from the theory of shallow-water equatorially trapped waves [*Matsuno*, 1966] are added on each spectrum for the different families of equatorial waves with equivalent depths of 12, 25, and 50 m.

4 Simulated Subseasonal Variability

4.1. Methodology

In this section, we compare the subseasonal variability simulated in the QOBS and QOBS+WP experiments in the six models. Building on the existing literature presented in the introduction, we focus mainly on the eastward propagating variability, examining in particular the presence/absence of convectively coupled Kelvin wave- (KW-) and MJO-like modes in the two aquaplanet experiments with and without a warm pool. The comparison is based on the different diagnostics of the subseasonal variability described below:

Figure 6 gives time-longitude plots (hovmoellers) of the 10° S–10° N averaged OLR anomaly relative to the time-mean value. No prefiltering is applied on the data so that variability on all time scales is kept. All the models have been run for 4 years or longer, but for sake of clarity and brevity each hovmoeller shows only 1 year of simulation, as an example representing the overall behavior of the given model.

Space-time coherence squared spectra of OLR and 850 zonal wind are computed following a similar method as in *Waliser et al*. [2009] and *Wheeler and Kiladis* [1999]. The method is applied here on overlapping 120 day time-segments covering the last 3 years of each simulation. For reference, dispersion curves derived from the theory of shallow-water equatorially trapped waves [*Matsuno*, 1966] are added on each spectrum for the different families of equatorial waves, using parameters that fit the CCEWs observed in nature (equivalent depths of 12, 25 and 50 m [see *Wheeler and Kiladis*, 1999; *Kiladis et al*., 2009]). Figures 7 and 8 show the symmetric (with respect to the equator) and anti-symmetric components of the spectrum, respectively. Note that this kind of diagnostics based on zonal wind and OLR emphasize by construction some types of CCEWs more than others, e.g., Kelvin Waves (KWs) more than Mixte Rossby Gravity waves (MRGs), because of their respective distinctive wind patterns. For further reference we thus also show the symmetric and antisymmetric spectra from observational data in Figure 9 (zonal wind from ERA-interim reanalyses [*Dee et al*., 2013] and OLR from the NOAA OLR data set [*Liebmann and Smith*, 1996]).

The horizontal structure of the eastward propagating modes is presented in Figures 10 and 11. The unfiltered daily fields of OLR, 850 hPa winds, 850 hPa geopotential height, and precipitation, are regressed onto two different indices of convective activity [e.g., *Kiladis et al*., 2009]. These two convective indices are computed from space-time filtered OLR in order to examine separately the slowly propagating large-scale features and the faster smaller-scale ones (respectively: (zonal wavenumber 1–5; period 20–100 days) and (zonal wavenumber 1–15; period 2–17 days)), then spatially averaged in a 20°×10° box centered on the

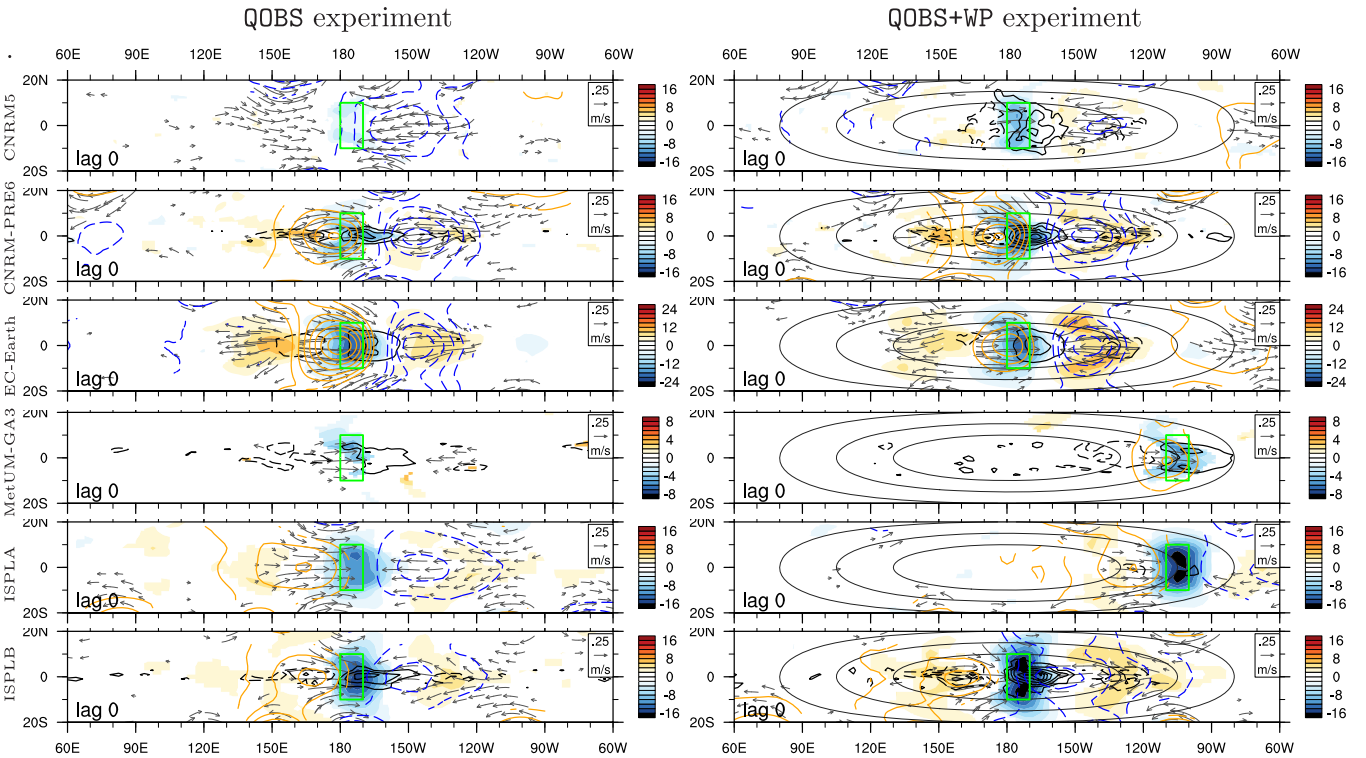

Figure 10. Horizontal structure of the high-frequency eastward propagating variability in the (left) QOBS and (right) QOBS+WP experiments in the 6 models. Unfiltered OLR (shading), 850 hPa winds (vectors), 850 hPa geopotential height (blue/orange contours), and precipitation (black contours) are regressed onto an index of convective activity computed from space-time filtered OLR (zonal wavenumber 1-15; period 2–17 days) spatially averaged in the green rectangle on the map (10° S-10° N;180° −190° E, or 250° −260° E for in the two cases where the variance was larger out of the warm pool). The regressed fields are plotted only at the gridpoints where the values pass the significance test (gridpoint t-test at the 0.05 level), and are otherwise set to zero. Precipitation anomalies are contoured every 1 mm d^{-1} in CNRM-5, IPSL-A, IPSL-B, every 2 mm d^{-1} in CNRM-PRE6 and EC-Earth, and every 0.5 mm d^{-1} in MetUM-GA3. Geopotential height anomalies are contoured every 0.5 m for all models except MetUM-GA3 (every 0.25 m).

equator, where the variance is the largest. The regressed fields are plotted only at the gridpoints where the values pass the significance test (gridpoint t-test at the 0.05 level), and are otherwise set to zero.

4.2. Zonally Symmetric Experiment (QOBS)

Five of the six models (all but CNRM-5) show OLR anomalies propagating eastward at about ∼10–15 m s^{-1} in the hovmoellers (Figure 6). The corresponding spectral peaks of at least three of them (CNRM-PRE6, EC-Earth, METO) lie along dispersion lines consistent with observed convectively coupled Kelvin waves (Figure 8), even if differences among the models remain in the amplitude, phase speed and frequency characteristics. The regressed horizontal structures at 850 hPa (Figure 10) are overall consistent with the structure of observed KWs [e.g., *Kiladis et al.*, 2009], with zonal wind anomalies on the equator, increased convection and precipitation signal collocated in the convergence, and almost no meridional wind anomaly, nor vorticity anomaly on either side of the equator.

As seen from its hovmoeller (Figure 6), CNRM-5 is the only model that does not produce any substantial eastward propagating OLR anomalies in the zonally symmetric configuration. Some eastward power is seen on the wind-OLR coherence squared spectrum (Figure 8) but it lies along a dispersion line of faster propagation and for shorter periods (2–4 days) than typical observed KWs. Furthermore, the regressed horizontal structure corresponding to this spectral peak highlights a significant dynamical signal (zonal wind and geopotential height anomalies in quadrature of phase), with only a very weak OLR anomaly and no significant precipitation (CNRM-5, Figure 10). This tends to suggest that this model produces KWs only very weakly coupled with convection. Note however that the newer version of this model (CNRM-PRE6), in which an entirely new package of moist-process parameterizations has been incorporated, does simulate KWs with phase-speed and horizontal characteristics much closer to the observations. In particular this new package includes a deep-convection scheme based on CAPE closure rather than moisture convergence, and implicitly take into account convective inhibition (CIN) through buoyancy in the updraft vertical velocity equation

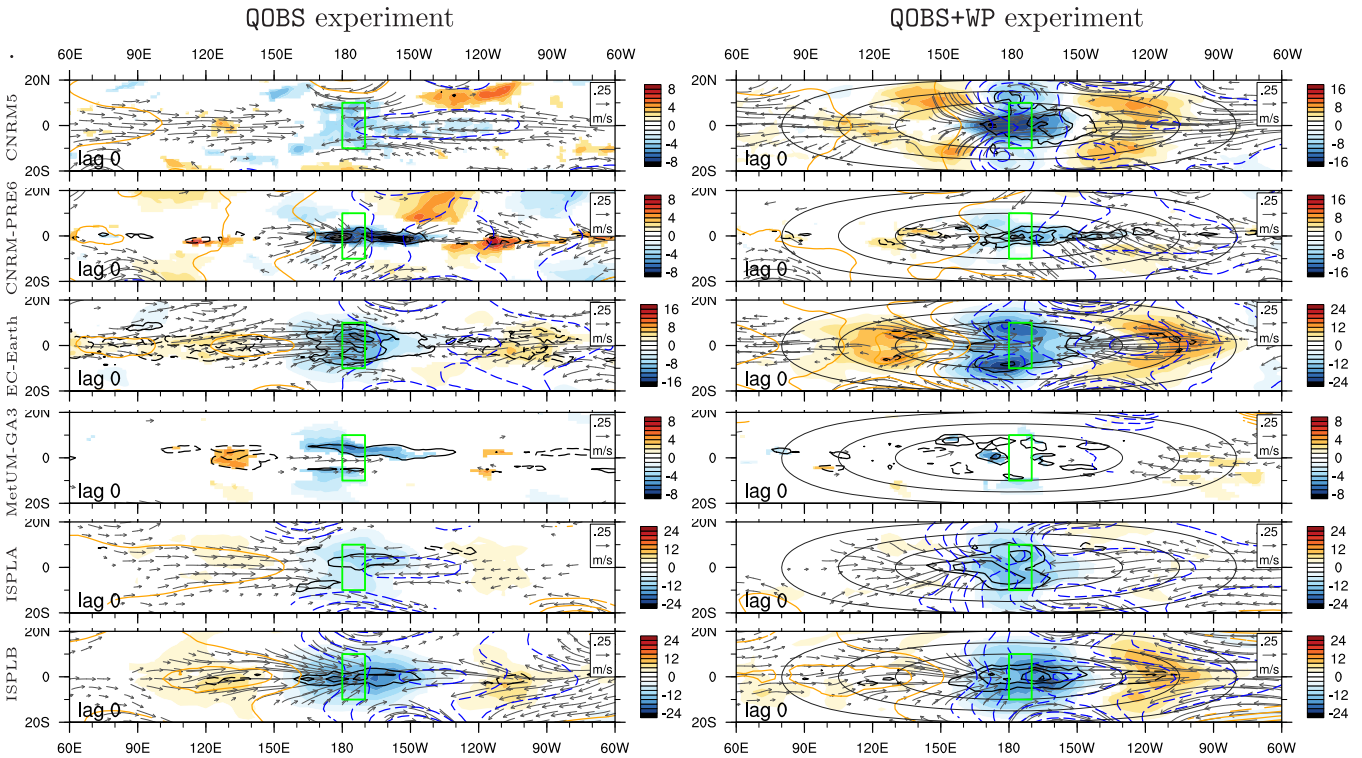

Figure 11. Same as Figure10 but for the low-frequency, low wave-number eastward propagating variability: the index of convective activity is computed from space-time filtered OLR (zonal wavenumber 1-5; period 20–100 days) spatially averaged in the green rectangle on the map (10° S-10° N;180° −190° E). Precipitation anomalies are contoured every 2 mm d^{-1} except in IPSL-A QOBS+WP (every 1 mm d^{-1}), and in IPSL-A QOBS, and MetUM-GA3 (every 0.5 mm d^{-1}). Geopotential height anomalies are contoured every 1 m except for CNRM-5 QOBS (every 2 m), IPSL-A QOBS (every 0.5 m) and MetUM-GA3 QOBS+WP (every 0.25 m).

[*Guérémy*, 2011]. This is consistent with recent theory suggesting the importance of convective inhibition to convectively coupled KWs [e.g., *Herman et al*., 2016].

Concerning the presence of MJO-like variability, our results tend to be consistent with the earlier conclusions from APE and *Maloney et al*. [2010] (with different models): we do not obtain any substantial MJO variability from any of the models in the zonally symmetric experiment. Note however that in half of the models, some slow OLR anomalies are seen propagating eastward at less than 5 m s^{-1}, in the form of faint wave-packets or "envelopes" of increased higher-frequency-wave activity with an irregular occurrence (Figure 6: MetUM-GA3, IPSLA, IPSLB). These slow eastward OLR anomalies are located in the eastern edge of the eastward equatorial zonal wind anomalies (Figure 11), but the resemblance with an observed MJO structure remains otherwise quite poor at this stage. In particular, the wind anomalies appear mostly zonal, as in a Kelvin wave, while cyclonic and anticyclonic vortices would be expected respectively behind and ahead of the convective signal in the case of an observed MJO. Besides, the existence of these large-scale intraseasonal zonal wind anomalies propagating around the equator cannot be taken alone as evidence of a MJO-like moisture mode, as they are known to also exist in dry idealized GCM experiments with no moisture prognostic equation [e.g., *Lin et al*., 2007]. A similar zonal wind pattern is in fact seen in all our models (Figure 11), even in those models where no clear associated OLR signal can be detected from the hovmoellers (Figure 6: CNRM-5, CNRM-PRE6, EC-Earth).

4.3. Warm-Pool Experiment (QOBS+WP)

From the hovmoellers in Figure 6, the impact of adding the warm pool on the tropical variability is hardly noticeable in two of the models, CNRM-PRE6 and IPSL-B. Note that those two also happen to be the two models with the narrowest ITCZs (Figure 3), and very little impact on the mean wind and precipitation when adding the warm pool. For the four other models, adding the warm pool has concentrated the largest OLR anomalies over the warm pool, and has modified the spatiotemporal organization of the tropical variability, in that some larger and lower-frequency OLR signal now arises in the warm-pool region in addition to KWs (if the latter exist in experiment QOBS).

In CNRM-5 and EC-Earth, the low frequency OLR signal arising over the warm pool is clearly propagating eastward at a phase speed of about 5 m s^{-1}. Interestingly, we find that these features propagate only in the warm pool and die off at its eastern edge, suggesting that some local elements of the mean state, specific to the warm pool, is necessary to trigger and sustain these disturbances in these models. The eastward propagation is less obvious from the hovmoellers and the spectra in MetUM-GA3 and IPSL-A. The regressed horizontal structures shown in Figure 11 for these four models still exhibit general patterns more consistent with an observed MJO than what could be seen in the QOBS experiment. In particular, vorticity anomalies symmetric about the equator are now seen accompanying the equatorial zonal wind signal (to various degrees depending on the models). See for example CNRM-5, where a pair of cyclonic vortices stands on both sides of the westerly wind anomaly at 850 hPa. The increased convective activity is located on the edge of the westerly wind anomaly, just west of the convergence, and a pair of anticyclonic vortices symmetric about the equator are also seen ahead of the convective anomaly.

We find that in the models where an intraseasonal eastward mode arises in the warm pool, this mode comes in addition to the faster KWs when those already existed in the zonally symmetric experiment. For example, both KWs and MJO-like modes are seen propagating at the same time in the warm pool in the EC-Earth hovmoeller, and they show distinct regressed horizontal structures (Figures 10 and 11). This indicates that some conditions do appear within the warm-pool environment that favors the growth of the intraseasonal MJO-like mode, and it is not just the result of a local phase-speed reduction of preexisting KWs. The case of CNRM-5, that simulates KWs very poorly in both experiments, but shows a strong MJO-like mode in the warm-pool experiment, also supports this conclusion. This finding brings an interesting modeling counterpoint to the idea developed in *Roundy* [2012] that the dynamics of observed KWs and MJO might overlap since their respective spectral signals are seen to overlap in observations.

As it appears, our results do not confirm a consistent behavior among the six models examined here concerning their ability to produce MJO-like variability in the warm-pool experiment. We find that an MJO-like variability only arises clearly in two models over six. In two other models, the warm pool does induce noticeable changes in the organization of convection, but the arising larger-scale anomalies are less organized in space and time. In the two remaining models, the impact of the warm pool could hardly be seen. In other words, the presence of a warm pool might be a necessary condition for a MJO-like moisture mode to arise [as hypothetized in, e.g., *Maloney et al*. [2010]), but based on the contrasting behaviors of our set of models, it does not seem to be a sufficient condition.

4.4. Additional Sensitivity Experiments

A few additional aquaplanet experiments have been conducted to test further the sensitivity of models behavior to the SST boundary conditions. The detailed results are not shown here for sake of brevity, but we give a summary of the main conclusions.

A first sensitivity experiment was performed with the six models to test the effect of a intermediate-size warm pool in the longitudinal direction (half-length $\Lambda_{lon}=50^o$ in longitude, and unchanged latitudinal width). Consistent with the results from experiment QOBS+WP ($\Lambda_{lon}=150^o$) presented in section 4.3, the intermediate-size warm pool induces modifications of the spatio-temporal organization of simulated tropical variability, with a confirmed tendency toward more intense, larger-scale and lower-frequency convective anomalies. It also confirmed that these modifications remain confined within the warm pool region. But as a consequence of the smaller longitudinal extension of the warm pool in this case, the developing larger-scale OLR anomalies do not have the space nor time to really propagate over the warm pool. Using a larger-size warm pool, such as the one we have used in experiment QOBS+WP ($\Lambda_{lon}=150^o$), appears to be more informative about whether a model is able to propagate large-scale OLR anomalies that might arise in the warm pool.

The effect of a more extended warm pool in longitude ($\Lambda_{lon}=180^o$, and unchanged latitudinal width) was investigated with only one model (CNRM-5). In this experiment, we find that the equatorial weakening of the low-level easterlies extends further in longitude compared to QOBS+WP ($\Lambda_{lon}=150^o$), but the low-level westerlies are weaker, and of similar longitudinal extension as in QOBS+WP. Propagating MJO-like anomalies arise in the large warm pool as in QOBS+WP, and those remain mostly confined to the center of the warm pool.

An additional experiment was also performed with CNRM-5 to test whether a zonally varying SST forcing (i.e., presence of the warm pool) was a necessary condition for this model to simulate MJO-like variability, or

whether it was just due to the locally warmer SST. This experiment used zonally uniform, warmer SST boundary conditions that peaked at the same temperature as the maximum SST in experiment QOBS+WP (i.e., T_{max}29° C). In this simulation, we find that the MJO-like mode does not develop. This confirms that a warm-pool-like zonally varying SST forcing is a necessary condition for CNRM-5 to simulate this mode.

4.5. Comparison Between CMIP, AMIP, and Aqua-Planet Configurations

As a complement to the spectra from our aquaplanet experiments, we also present in Figures 8 and 9 the spectra computed from the corresponding AMIP and CMIP simulations of each model performed and made available for CMIP-5. The CMIP simulation with model CNRM-PRE6 is missing on the figures because this model is currently being developed for the coming CMIP-6, and only the AMIP simulation was available at the time of our study. The CMIP and AMIP spectra have been computed over a period of three full years, for consistency with the aquaplanet spectra. To our knowledge this is the first time that a cross-comparison is presented of space-time spectra for both a set of different GCMs using various parameterization schemes, and four configurations of each model: CMIP, AMIP, zonally symmetric aquaplanet, and aquaplanet with a warm pool.

For both the symmetric and anti-symmetric components, the amplitude of the various CCEW spectral peaks is larger in the aquaplanets than in the corresponding AMIP and CMIP spectra, likely because the aquaplanets simulate less background noise than the more realistic configurations. Apart from that, we find that most peaks align along equivalent depths (i.e., phase speeds) that are consistent across the different configurations of a given model. There is more consistency in the spectra for a given model across its four configurations, than for a given configuration across the six models. For example, the spectral peak of the too fast and weakly coupled KWs in CNRM-5 aquaplanet (cf. section 4.2) is also seen in both its AMIP and CMIP configurations. Note also the good consistency between CMIP, AMIP, QOBS and QOBS+WP regarding Mixed Rossby-Gravity waves (MRGs) on the antisymmetric spectra (Figure 9: EC-Earth, CNRM-PRE6, CNRM-5).

This finding that simulated CCEW characteristics remain relatively consistent across configurations highlights again the primary influence of the parameterization choices on simulated CCEWs, compared to mean-state influence or other effects. This is consistent with results based on observational data from *Dias and Kiladis* [2014], showing only a weak influence of the background state on modulating the dispersion properties of convectively coupled equatorial waves. Our result also argues in favor of using aquaplanet experiments to investigate further, at cheaper numerical costs, the behavior of a given model and test for example the effect of different parameterization schemes or parameters on simulated CCEWs.

Note that in the case of KWs, the similarity of phase speed across configurations tends to echo the work of *Frierson et al*. [2011]. They showed that, to the first order, the phase speed (equivalent depth) of the KWs simulated in several AMIP-like GCMs was linked to the time-mean Gross Moist Stability, which is itself closely dependent on the type of parameterization scheme used for deep convection. In fact, this aspect will be investigated further in the discussion section.

As opposed to the consistency seen for CCEW characteristics, the spectral signature of MJO-like variability can change significantly across configurations for a given model (Figure 8). This is not really a surprising result since a few GCMs are already known to show very different behaviors in their CMIP and AMIP configurations. CNRM-5 in particular, is known to produce an MJO mode of large amplitude in its coupled (CMIP) configuration but a much weaker and less propagating variability in its forced (AMIP) configuration [e.g., *Jiang et al*., 2015]. Note that in our aquaplanet experiments, the MJO-like mode simulated in CNRM-5 QOBS+WP is switched on and off with only a change of spatial geometry of the *forced* SST. This would tend to suggest that the absence of interactive ocean in the full AMIP configuration is not necessary the main factor to explain its weak MJO compared to CMIP. Differences in the mean state between AMIP and CMIP might actually play a crucial role. In fact, a recent study by *Jiang et al*. [2015] showed that both the mean state and the interactive coupling play a role in the MJO-like variability simulated in CNRM-5. They performed a modified-AMIP experiment, where the SST boundary condition was taken from the CMIP experiment. They found that the tropical mean state in the modified-AMIP experiment was very close to the mean state of the CMIP experiment, and yet the simulated MJO-like variability had intermediate characteristics between the MJO simulated in the original-AMIP and the CMIP experiments. This question of the relative role of coupling and mean state remains open and could benefit from further investigations in aquaplanet configuration with interactive coupling with an idealized ocean such as one-dimension mixed layer ocean model [e.g., *Klingaman and Woolnough*, 2014] and as proposed in the upcoming intercomparison project: TRAC-

MIP (Tropical rain belts with an Annual cycle and a Continent Model Intercomparison Project: http://www.wcrp-climate.org/gc-clouds-circulation-activities/gc4-clouds-initiatives/).

5. Discussion

The impact of adding a warm pool on the tropical mean state and the subseasonal variability has been documented separately in sections 3 and 4. In this section, we now investigate whether our set of experiments gives support to potential links between the tropical variability and the mean state that have been discussed in previous literature.

5.1. Mean Low-Level Equatorial Westerly Winds

One aspect discussed in existing literature is the importance of the absolute westerly winds in the warm-pool region to sustain the eastward propagation of intraseasonal moisture modes. *Sobel and Maloney* [2012] proposed a theoretical framework in which large-scale tropical moisture anomalies can grow and propagate eastward through advection of anomalous humidity by the sum of perturbation winds and mean westerly flow background. The importance of the mean low-level westerlies for eastward propagation was also supported by *Maloney et al*. [2010]. Based on a series of aquaplanet sensitivity experiments, they found that, in their model, reducing the lower-troposphere westerly flow in the warm pool by reducing the zonal SST gradient had the effect of slowing and weakening the eastward propagation of their intraseasonal moisture mode. They point out the effect of the mean state on the sign of surface flux anomalies relative to convection in their model, with positive surface flux anomalies occurring near and to the west of MJO convection, and helping to destabilize the MJO.

Our set of aquaplanet experiments shows that these moisture processes and the relative importance of the different terms in the anomalous moisture budget are not necessarily the same in all the models. First consider CNRM-5: consistent with *Maloney et al.*'s [2010] results, the development of MJO-like variability over the warm pool coincides with the simulation of significant mean low-level equatorial westerly winds in the experiment QOBS+WP. On the other hand, only very weak mean westerly winds are seen in experiment QOBS+WP with EC-Earth but this model also simulates a decent MJO-like variability. Experiment QOBS+WP with IPSL-A provides a third example, in which mean westerly winds are produced over the warm pool, with an amplitude and longitude extension relatively similar to the westerly winds in CNRM-5, but yet no MJO variability arises. In other words, in our set of models, the presence, amplitude or longitudinal extent of the mean low-level westerly winds over the warm pool are not sufficient criteria to discriminate the ability of a model to simulate MJO-like variability. Similarly, we have not found any consistent link either with the vertical shear of the zonal wind over the warm pool (e.g., Figure 5).

5.2. Time-Mean Export of the Vertically Integrated Moist Static Energy

The way each model can simulate convectively coupled modes in the tropics is strongly linked with how subgrid scale moist convective processes are represented in this given model, and how the balance between the convective forcing and the large-scale flow is reached, with all the intervening feedbacks between moist processes and circulation. Integrated thermodynamical quantities such as the Gross Moist Stability (GMS) [*Neelin and Held*, 1987; *Raymond et al*., 2009] are often derived in an attempt to diagnose and quantify this complex balance. The Gross Moist Stability measures the export of Moist Static Energy (MSE), or of moist entropy, from an atmospheric column, in a convective overturning circulation per unit of mass transport. *Benedict et al*. [2014] found a linear correlation between time-mean normalized GMS and the ability of a set of AMIP simulations to produce an MJO, the models with weaker (positive) GMS showing a better eastward propagation of intraseasonal MJO-like disturbances. They also showed that this correlation was mainly due to the contribution from vertical advection to the GMS, with a smaller contribution from horizontal advection. A link between the time-mean GMS and the equivalent depth (or phase speed) of convectively coupled KWs simulated in several versions of an AGCM was also suggested in *Frierson et al*. [2011].

Does our set of models support the idea that the time-mean export of MSE in a model can reflect and inform on the way this model simulates tropical convectively coupled modes? To investigate this question, we focus here on comparing the time-mean export of vertically integrated MSE (i.e., the nonnormalized GMS) from three of our models with contrasting behaviors regarding MJO and KW variability: CNRM-5, CNRM-PRE6, EC-Earth.

The export of MSE integrated over the column from the surface to the top of the atmosphere is expressed as $\nabla \cdot \langle h\mathbf{v} \rangle$, where $\mathbf{v}$ is the horizontal wind, and where $\langle \cdot \rangle$ stands for the vertical mass integral from the surface to the top of the atmosphere. h is the MSE: $h = c_p T + gz + L_v q_v$ where c_p is the heat capacity, T the temperature, g the acceleration of gravity, z the altitude, L_v the latent heat of vaporization and q_v the specific humidity. In each model, $\nabla \cdot \langle h\mathbf{v} \rangle$ is balanced by the surface latent and sensible heat fluxes (LH, SH) and radiative flux divergence between the surface and the top of the atmosphere (short-wave SW and long-wave LW) in the MSE full budget equation [see e.g., *Raymond et al*., 2009]:

$$\frac{\partial \langle h \rangle}{\partial t} + \nabla \cdot \langle h\mathbf{v} \rangle = LH + SH + LW + SW \tag{1}$$

Building on the existing literature mentionned previously, we focus here on the time-mean export term $\nabla \cdot \langle h\mathbf{v} \rangle$, and we further decompose it into its components related to horizontal and vertical advection:

$$\nabla \cdot \langle \overline{h\mathbf{v}} \rangle = \langle \overline{\mathbf{v} \cdot \nabla h} \rangle + \langle \overline{h \nabla \cdot \mathbf{v}} \rangle = \left\langle \overline{u \frac{\partial h}{\partial x} + v \frac{\partial h}{\partial y}} \right\rangle + \left\langle \overline{\omega \frac{\partial h}{\partial p}} \right\rangle \tag{2}$$

where u,v are the zonal and meridional components of the horizontal wind, p is the pressure, ω is the vertical pressure velocity, and overbars denote time averaging The time mean was computed from the daily product terms: $u\frac{\partial h}{\partial x} + v\frac{\partial h}{\partial y}$ (horizontal advection) and $\omega \frac{\partial h}{\partial p}$ (vertical advection), then integrated over the vertical.

The resulting time-mean terms are mapped in Figure 12 for AMIP simulations, and in Figures 13 and 14 for aquaplanet experiments. The time-mean terms from the AMIP simulations is computed over 3 years only, for consistency with the aquaplanet experiments. For reference, Figure 12a also shows these three terms computed from reanalysis ERA-interim (ERA-i) [*Dee et al*., 2013]. The reanalysis product shows an export of MSE mainly positive in the precipitating areas (as indicated by the time-mean precipitation contours), except in the eastern pacific equatorial region. Where convection is the most intense, along the equator in the Indian ocean, maritime continent and western Pacific, both the terms from the vertical and horizontal advection are positive, with the vertical advection term slightly dominant. Note that there is good consistency in the patterns and amplitude with *Benedict et al*.'s [2014] corresponding figure, for which they have computed the GMS terms from the moist entropy budget (instead of MSE budget here). In comparison, the total export of MSE within the ITCZ in the `QOBS` experiment is positive in EC-Earth but weakly negative in CNRM-5 and CNRM-PRE6 (Figures 13 and 14). This weakly negative total export results from the sum of opposite-sign contributions from vertical and horizontal advections in both CNRM-5 and CNRM-PRE6 models, while in EC-Earth the two contributions are positive as in the reanalysis. Note however that EC-Earth and ERA-i are not fully independent since the production of the latter makes use of an AGCM (the Integrated Forecasting System IFS) of the same family as EC-Earth.

Over the warm pool (experiment `QOBS+WP`), the total export of MSE is always increased compared to the zonally symmetric case. But again, in CNRM-5 and CNRM-PRE6, the vertical and horizontal components are of opposite sign and the horizontal term dominates, yielding a net export, while both terms are positive in EC-Earth. We find that the MJO-like mode is simulated by the two models with the most intense time-mean total export of MSE from the warm-pool region (CNRM-5 and EC-Earth), while the model with weak MSE export from the warm-pool region does not simulate MJO-like variability (CNRM-PRE6). This remains true when considering the normalized GMS spatially averaged over the warm pool (not shown) and thus differs from *Benedict et al*.'s [2014] findings. Note also that the relative roles of the contributions from the horizontal and vertical advections is different in CNRM-5 and EC-Earth: the intensification of the total advection in the warm pool is mainly due to an increase of the contribution from horizontal advection in CNRM-5 (the contribution from vertical advection remain negative), while it is due to an increase of both contributions in EC-Earth (and in particular the contribution from vertical advection). In other words, these results shows that the interaction between convection and large-scale flow involves different mechanisms in these two models, resulting in a different balance between transport and in-column processes, but with the same net effect on the net column export of MSE in the warm-pool region.

It is however noteworthy that we find again a relatively good consistency between the AMIP, CMIP and aquaplanet simulations of each model. The MSE export terms for the AMIP simulations of the same three models as above is shown in Figure 12 (the terms from the CMIP simulations are not shown here for sake of brevity as they are very similar to the AMIP ones). In the equatorial region from Indian ocean to west Pacific,

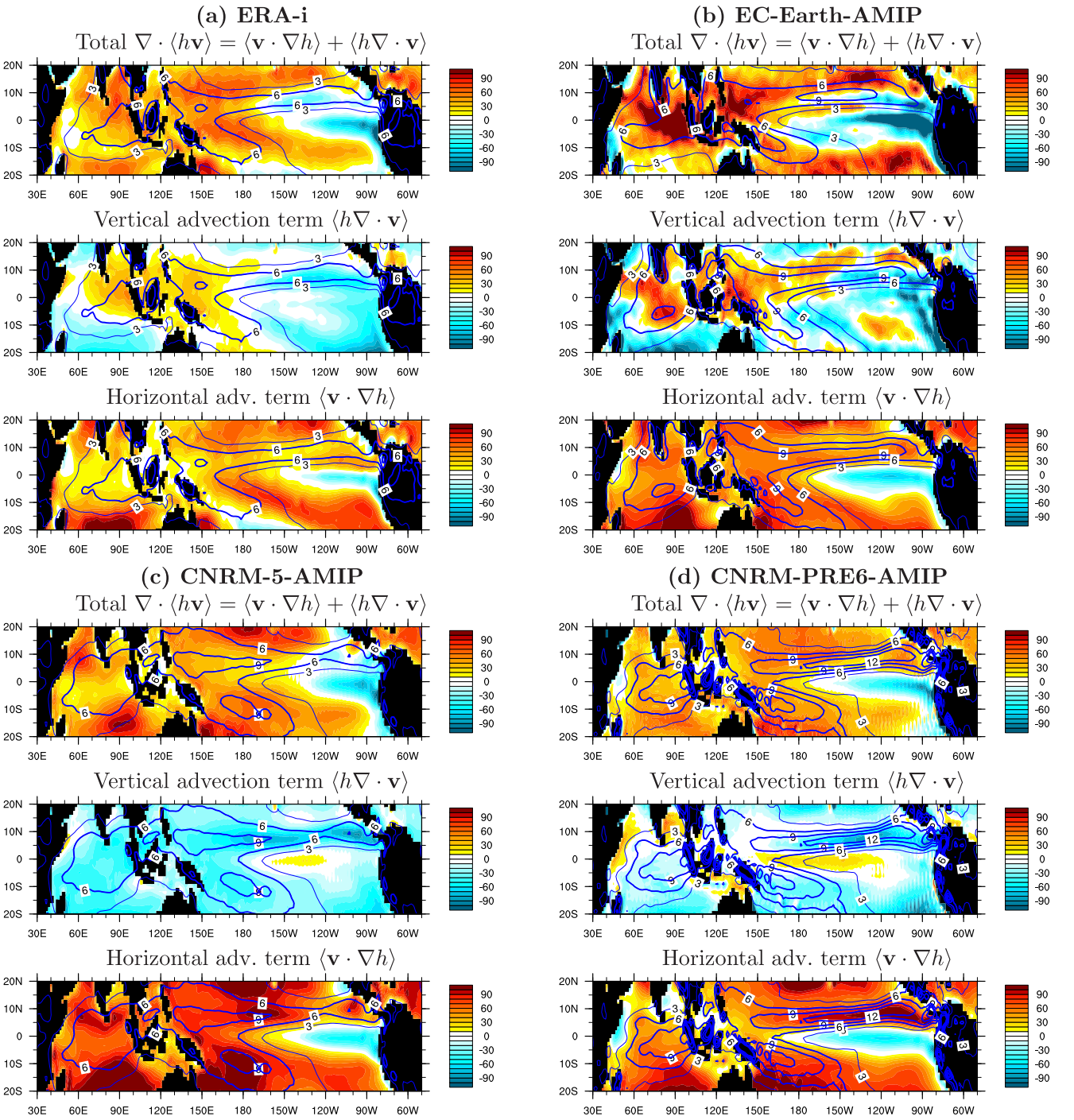

Figure 12. Time-mean export of MSE $\nabla \cdot \langle \overline{h\mathbf{v}} \rangle$ in W m^{-2} and contributions from the vertical and horizontal advection, calculated from (a) monthly output of ERA-i, (b) daily outputs of EC-Earth-AMIP, (c) daily outputs of CNRM-5-AMIP, and (d) daily outputs of CNRM-PRE6-AMIP. Time-mean precipitation is contoured in mm d^{-1}.

the total export of MSE in CNRM-5-AMIP and CNRM-PRE6-AMIP result from the sum of opposite-sign contributions, with a negative contribution from vertical advection, as it is the case over the warm pool in the corresponding experiments QOBS+WP. On the contrary, both contributions are positive in EC-Earth-AMIP, consistently with the corresponding experiment QOBS+WP. This consistency confirms the potential usefulness of using idealized aquaplanet experiments to document the interaction between moist processes and circulation in a given AGCM and to evaluate parameterization schemes. This also promotes the use of similar aquaplanet simulations to study at a reduced computational cost the response of the atmospheric

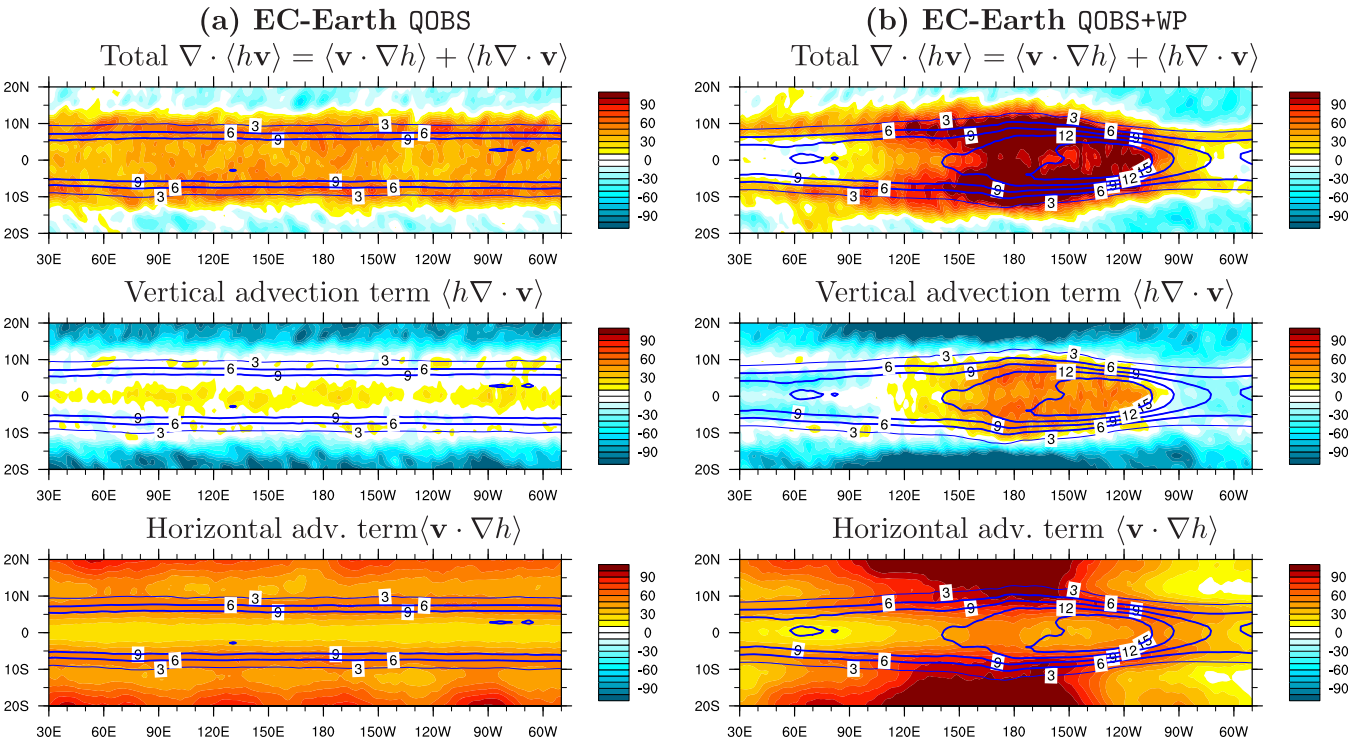

Figure 13. Time-mean export of MSE $\nabla \cdot \langle \overline{h\mathbf{v}} \rangle$ in W m^{-2} and contributions from vertical and horizontal advection, calculated from daily outputs of EC-Earth (a) QOBS and (b) QOBS+WP aquaplanet experiments. Time-mean precipitation is contoured in mm d^{-1}.

circulation to a warming climate [e.g., *Voigt and Shaw*, 2015], but emphasizes at the same time the importance of a multimodel approach.

Investigating further the mechanisms by which each of the models reaches a balance between convection and large-scale transport over the warm pool would be beyond the scope of the current study and will be left for future work. But a logical perspective could indeed be to compute and analyze the full budget of MSE in each model, both for the time-mean and MJO-anomaly components. In regard of previously reported results [e.g., *Hannah and Maloney*, 2014], it would probably be particularly useful to compare the relative role of the right-hand side terms, radiative and surface heat flux feedbacks, in balancing the vertical and horizontal advection terms. Given the inter-model diversity seen in our results here for both the tropical variability and the mean state (especially in Figures 12–14), it is likely that such analysis will confirm a diversity of mechanisms at play, but this would nevertheless be useful information to know for each modeling group.

6. Summary and Concluding Remarks

This study compares the simulation of subseasonal tropical variability by a set of six AGCMs in two experiments in aquaplanet configuration: a zonally symmetric experiment, and an experiment with a warm pool centered on the equator. This framework focuses the comparison on the effect of the models' parameterizations and mean states, excluding by design other factors such as land-sea contrasts, seasonality, etc. Overall, we find that despite this simplified framework, diversity clearly remains among the models, both in the response of the mean state to the warm pool and in the simulated tropical subseasonal variability.

This diversity is already evident in the time-mean tropical circulation and precipitation patterns simulated by the different AGCMs in the reference experiment QOBS. In all the models, adding the warm pool in the SST boundary conditions induces zonal asymmetries in the simulated mean states in the form of a "Gill-type" response [*Gill*, 1980]. This response is however made more complex in our case due to model-specific interactions between moisture, convective heating and circulation. Noticeable variations appear from one model to another. And we find that only half the models simulate mean low-level equatorial westerlies over the warm pool as in *Maloney et al.* [2010].

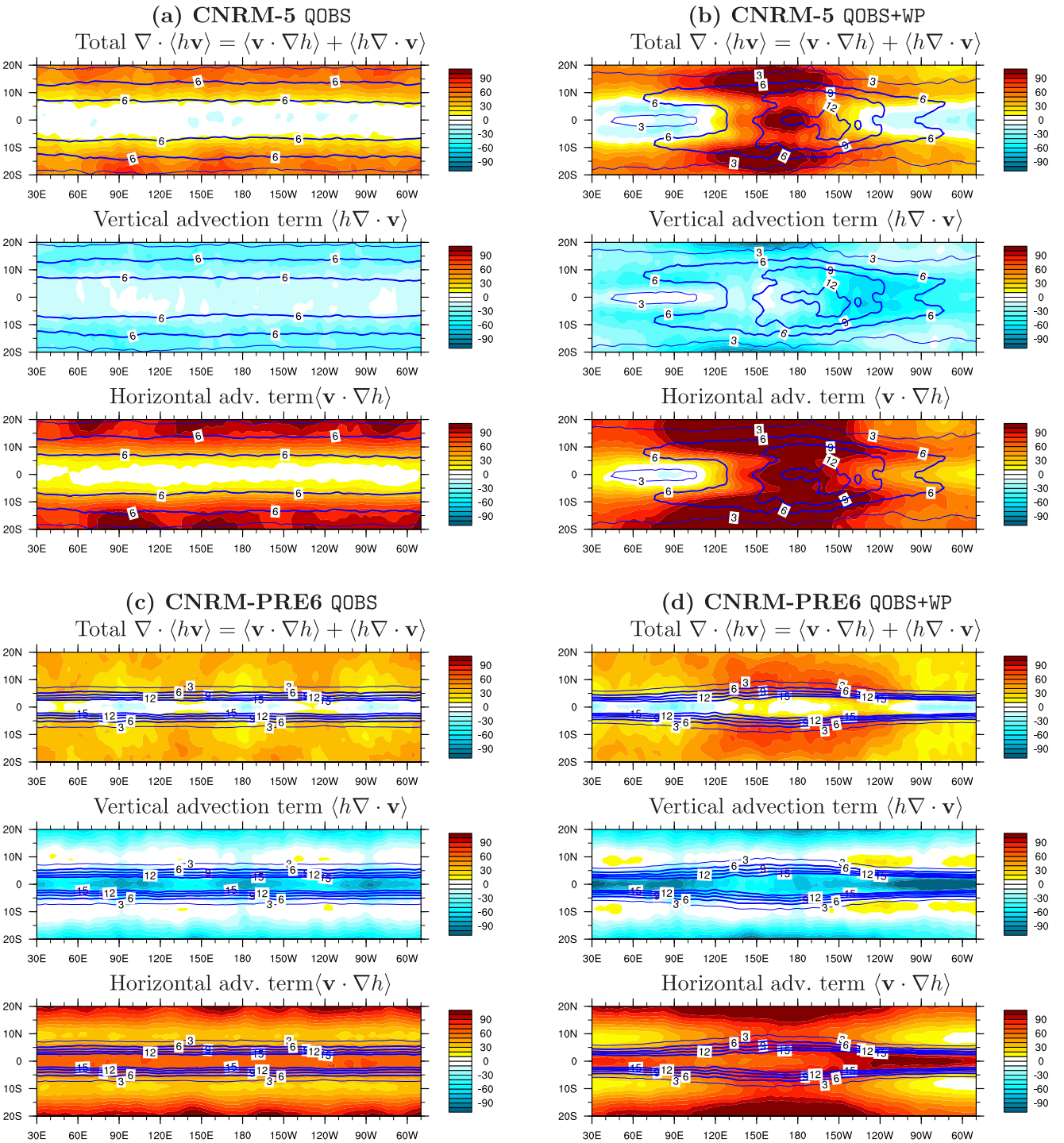

Figure 14. Time-mean export of MSE $\nabla \cdot \langle \overline{h\mathbf{v}} \rangle$ in W m^{-2} and contributions from vertical and horizontal advection, calculated from daily outputs of (a) CNRM-5 QOBS, (b) CNRM-5 QOBS+WP, (c) CNRM-PRE6 QOBS, and (d) CNRM-PRE6 QOBS+WP aquaplanet experiments. Time-mean precipitation is contoured in mm d^{-1}.

The CCEWs simulated by the six models in the idealized aquaplanet configuration are also very diverse, and so is the ability of the models to produce MJO-like variability. In the zonally symmetric experiment (QOBS), we do not find any substantial MJO variability in any of the models, and this is consistent with the earlier conclusions from APE and *Maloney et al.* [2010]. For about half the models, the addition of a warm pool clearly favors the development of a large-scale variability relatively consistent with observed MJO characteristics. This large-scale intraseasonal variability comes in addition to CCEWs, that remains broadly similar in

both experiments QOBS and QOBS+WP. The other half of models do not simulate MJO-like variability even over a warm pool, demonstrating that a warm pool is not a sufficient condition for this type of variability to arise. However, we also find that, in the models where an MJO-like mode develops, it remains confined over the warm pool, which must then be locally providing the favorable and necessary conditions for its growth.

The inter-model differences that we have been examining here can only arise from the simulated interaction between subgrid processes and grid-scale dynamics. The dynamical cores of AGCMs are thought to be fairly equivalent: they solve the same fundamental equations (i.e., the primitive equations) and differ mostly by their numerics. The differences between models arise mostly from the representation of subgrid processes, and particularly cloud processes. Aquaplanet configurations appear sufficient to shed some light on these inter-model differences, and present clear advantages in terms of computational cost and ease of analysis compared to more realistic configurations. One limiting factor in the use of such configurations, however, is the lack of an observed "aquaplanet" reference. An interesting alternative could be to include in future aquaplanet inter-comparison studies a reference aquaplanet simulation with explicitly resolved convection. Such models (CRM, convection-resolving models) are computationally expensive but they provide a wealth of information that could not be directly observed, and some short simulations are already available [*Bretherton and Khairoutdinov*, 2015]. Alternative approaches could also be considered to reduce the computational cost, such as using "reduced-planet" models [e.g., *Semane and Bechtold*, 2015]. Note however that such simulations with explicitly resolved convection would still remain dependent on parametrized microphysics and boundary layer processes, influencing in turn the radiative feedback terms.

The inter-model comparison was combined in this study with a comparison across configurations for each model. We have documented the space-time coherence squared spectra from CMIP, AMIP, QOBS, and QOBS+WP experiments for each of the six models. One noteworthy result is the remarkable consistency of the CCEWs characteristics of a given model across its different configurations, from fully coupled (CMIP) to zonally symmetric aquaplanet. Similar consistency across configurations is not found for MJO variability, but it was also found in time-mean quantities like the Gross Moist Stability, which provide an integrated measure of the balance reached in a model between the effects of moist processes and the large-scale flow. The present study suggests that not all models necessarily reach this balance via the same mechanisms, consistent with what other studies also imply [e.g., *Hannah and Maloney*, 2014; *Benedict et al*., 2014; *Jiang et al*., 2015; *Klingaman et al*., 2015; *Xavier et al*., 2015]. Multimodel aquaplanet experiments makes an interesting framework to investigate further the behavior of new parameterization schemes and intercomparing models at a reduced computational cost. Additional degrees of complexity could also be progressively put back in the experimental design, to study separately the relative influence of other factors on simulated tropical subseasonal variability. It would be particularly interesting to investigate how seasonal effects (e.g., off-equatorial warm pool, monsoon-like SST anomaly, time-varying seasonal radiative forcing), changes in the warm pool amplitude, or coupling to an interactive ocean (e.g., Tropical rain belts with an Annual cycle and a Continent Model Intercomparison Project: TRAC-MIP, http://www.wcrp-climate.org/gc-clouds-circulation-activities/gc4-clouds-initiatives/), might modulate the models behavior presented here for a time-independent, equinoctial and SST-forced setup.

Acknowledgments
We thank Juliana Dias, Eric Maloney and an anonymous reviewer for their constructive comments and suggestions that lead to substantial improvements in the manuscript. This work was funded by the European Commission's 7th Framework Programme, under grant agreement 282672, EMBRACE project (http://www.embrace-project.eu/). The aquaplanet experiments discussed in this paper can be made available upon request (contact: romain.roehrig@meteo.fr).

References

Andersen, J. A., and Z. Kuang (2012), Moist static energy budget of mjo-like disturbances in the atmosphere of a zonally symmetric aquaplanet., *J. Clim.*, *25*(8), 2782–280.

Benedict, J. J., E. D. Maloney, A. H. Sobel, and D. M. Frierson (2014), Gross moist stability and mjo simulation skill in three full-physics GCMs, *J. Atmos. Sci.*, *71*(9), 3327–3349.

Blackburn, M., and B. Hoskins (2013), Context and aims of the aquaplanet experiment, *J. Meteorol. Soc. Jpn.*, *91A*, 1–15.

Bougeault, P. (1985), A simple parameterization of the large-scale effects of cumulus convection, *Mon. Weather Rev.*, *113*(12), 2108–2121.

Bretherton, C. S., and M. F. Khairoutdinov (2015), Convective self-aggregation feedbacks in near-global cloud-resolving simulations of an aquaplanet, *J. Adv. Model. Earth Syst.*, *7*, 1765–1787, doi:10.1002/2015MS000499.

Cassou, C. (2008), Intraseasonal interaction between the madden–julian oscillation and the north Atlantic oscillation, *Nature*, *455*, 523–527.

Couvreux, F., et al. (2015), Representation of daytime moist convection over the semi-arid tropics by parametrizations used in climate and meteorological models, *Q. J. R. Meteorol. Soc.*, *141*(691), 2220–2236, doi:10.1002/qj.2517.

Dee, D. P., M. Balmaseda, G. Balsamo, R. Engelen, A. J. Simmons, and J. N. Thépaut (2013), Toward a consistent reanalysis of the climate system, *Bull. Am. Meteorol. Soc.*, *95*(8), 1235–1248, doi:10.1175/bams-d-13-00043.1.

DeMott, C. A., C. Stan, D. A. Randall, and M. D. Branson (2014), Intraseasonal variability in coupled GCMs: The roles of ocean feedbacks and model physics, *J. Clim.*, *27*, 4970–4995, doi:10.1002/qj.2517.

Dias, J., and G. N. Kiladis (2014), Influence of the basic state zonal flow on convectively coupled equatorial waves, *Geophys. Res. Lett.*, *41*, 6904–6913, doi:10.1002/2014GL061476.
Dufresne, J.-L., et al. (2013), Climate change projections using the ipsl-cm5 earth system model: From cmip3 to cmip5, *Clim. Dyn.*, *40*(9-10), 2123–2165.
Emanuel, K. A. (1991), A scheme for representing cumulus convection in large-scale models, *J. Atmos. Sci.*, *48*(21), 2313–2329.
Frierson, D. M., D. Kim, I.-S. Kang, M.-I. Lee, and J. Lin (2011), Structure of AGCM-simulated convectively coupled kelvin waves and sensitivity to convective parameterization, *J. Atmos. Sci.*, *68*(1), 26–45.
Gill, A. E. (1980), Some simple solutions for heat-induced tropical circulation, *Q. J. R. Meteorol. Soc.*, *106*(449), 447–462, doi:10.1002/qj.49710644905.
Gottschalck, J., et al. (2010), A framework for assessing operational Madden-Julian Oscillation Forecasts: A CLIVAR MJO Working Group Project, *Bull. Am. Meteorol. Soc.*, *91*(9), 247–1258, doi:10.1175/2010BAMS2816.1.
Grandpeix, J.-Y., and J.-P. Lafore (2010), A density current parameterization coupled with emanuel's convection scheme. Part I: The models, *J. Atmos. Sci.*, *67*(4), 881–897.
Gregory, D., and P. Rowntree (1990), A mass flux convection scheme with representation of cloud ensemble characteristics and stability-dependent closure, *Mon. Weather Rev.*, *118*(7), 1483–1506.
Guérémy, J. (2011), A continuous buoyancy based convection scheme: One-and three-dimensional validation, *Tellus, Ser. A*, *63*(4), 687–706.
Han, Y., and B. Khouider (2010), Convectively coupled waves in a sheared environment, *J. Atmos. Sci.*, *67*(9), 2913–2942, doi:10.1175/2010JAS3335.1.
Hannah, W. M., and E. D. Maloney (2011), The role of moisture–convection feedbacks in simulating the Madden–Julian Oscillation, *J. Clim.*, *24*(11), 2754–2770, doi:10.1175/2011JCLI3803.1.
Hannah, W. M., and E. D. Maloney (2014), The moist static energy budget in NCAR CAM5 hindcasts during dynamo, *J. Adv. Model. Earth Syst.*, *6*, 420–440, doi:10.1002/2013MS000272.
Hayashi, Y.-Y., and A. Sumi (1986), The 30-40 day oscillations simulated in an "aqua planet" model, *J. Meteorol. Soc. Jpn.*, *64*, 451–467.
Hazeleger, W., et al. (2012), EC-Earth v2. 2: Description and validation of a new seamless earth system prediction model, *Clim. Dyn.*, *39*(11), 2611–2629.
Herman, M. J., Z. Fuchs, D. J. Raymond, and P. Bechtold (2016), Convectively coupled kelvin waves: From linear theory to global models, *J. Atmos. Sci.*, *73*(1), 407–428.
Hess, P. G., D. S. Battisti, and P. J. Rasch (1993), Maintenance of the intertropical convergence zones and the large-scale tropical circulation on a water-covered earth, *J. Atmos. Sci.*, *50*(5), 691–713.
Hoskins, B., R. Neale, M. Rodwell, and G.-Y. Yang (1999), Aspects of the large-scale tropical atmospheric circulation, *Tellus, Ser. B*, *51*(1), 33–44.
Hourdin, F., et al. (2006), The LMDZ4 general circulation model: Climate performance and sensitivity to parametrized physics with emphasis on tropical convection, *Clim. Dyn.*, *27*(7-8), 787–813.
Hourdin, F., et al. (2013), LMDZ5B: The atmospheric component of the IPSL climate model with revisited parameterizations for clouds and convection, *Clim. Dyn.*, *40*(9-10), 2193–2222.
Hung, M.-P., J.-L. Lin, W. Wang, D. Kim, T. Shinoda, and S. J. Weaver (2013), MJO and convectively coupled equatorial waves simulated by CMIP5 Climate models, *J. Clim.*, *26*(17), 6185–6214.
Inness, P. M., J. M. Slingo, E. Guilyardi, and J. Cole (2003), Simulation of the Madden–Julian Oscillation in a coupled general circulation model. Part II: The role of the basic state, *J. Clim.*, *16*(3), 365–382.
Jiang, X., et al. (2015), Vertical structure and physical processes of the Madden-Julian Oscillation: Exploring key model physics in climate simulations, *J. Geophys. Res. Atmos.*, *120*, 4718–4748, doi:10.1002/2014JD022375.
Kang, I.-S., F. Liu, M.-S. Ahn, Y.-M. Yang, and B. Wang (2013), The role of SST structure in convectively coupled Kelvin-Rossby waves and its implications for MJO formation, *J. Clim.*, *26*(16), 5915–5930, doi:10.1175/jcli-d-12-00303.1.
Kiladis, G. N., M. C. Wheeler, P. T. Haertel, K. H. Straub, and P. E. Roundy (2009), Convectively coupled equatorial waves, *Rev. Geophys.*, *47*, RG2003, doi:10.1029/2008RG000266.
Klingaman, N., and S. Woolnough (2014), The role of air–sea coupling in the simulation of the Madden–Julian oscillation in the Hadley centre model, *Q. J. R. Meteorol. Soc.*, *140*(684), 2272–2286.
Klingaman, N. P., et al. (2015), Vertical structure and physical processes of the Madden-Julian oscillation: Linking hindcast fidelity to simulated diabatic heating and moistening, *J. Geophys. Res. Atmos.*, *120*, 4690–4717, doi:10.1002/2014JD022374.
Landu, K., and E. D. Maloney (2011), Effect of SST distribution and radiative feedbacks on the simulation of intraseasonal variability in an aquaplanet GCM, *J. Meteorol. Soc. Jpn.*, *89*(3), 195–210.
Liebmann, B., and C. A. Smith (1996), Description of a complete (interpolated) outgoing longwave radiation dataset, *Bull. Am. Meteorol. Soc.*, *77*, 1275–1277.
Lin, H., G. Brunet, and J. Derome (2007), Intraseasonal variability in a dry atmospheric model, *J. Atmos. Sci.*, *64*(7), 2422–2441, doi:10.1175/JAS3955.1.
Madden, R. A., and P. R. Julian (1972), Description of global-scale circulation cells in the tropics with a 40-50 day period, *J. Atmos. Sci.*, *29*(6), 1109–1123.
Maloney, E. D. (2009), The moist static energy budget of a composite tropical intraseasonal oscillation in a climate model, *J. Clim.*, *22*(3), 711–729, doi:10.1175/2008JCLI2542.1.
Maloney, E. D., A. H. Sobel, and W. M. Hannah (2010), Intraseasonal variability in an aquaplanet general circulation model, *J. Adv. Model. Earth Syst.*, *2*, 5, doi:10.3894/JAMES.2010.2.5.
Matsuno, T. (1966), Quasi-geostrophic motions in the equatorial area, *J. Meteorol. Soc. Jpn.*, *44*(1), 25–43.
Michou, M., P. Nabat, and D. Saint-Martin (2015), Development and basic evaluation of a prognostic aerosol scheme (v1) in the CNRM climate model CNRM- CM6, *Geosci. Model Dev.*, *8*(3), 501–531, doi:10.5194/gmd-8-501-2015.
Moore, R. W., O. Martius, and T. Spengler (2010), The modulation of the subtropical and extratropical atmosphere in the pacific basin in response to the Madden–Julian oscillation, *Mon. Weather Rev.*, *138*(7), 2761–2779, doi:10.1175/2010MWR3194.1.
Nakajima, K., Y. Yamada, Y. O. Takahashi, M. Ishiwatari, W. Ohfuchi, and H. Y.Y. (2013a), The variety of spontaneously generated tropical precipitation patterns found in ape results, *J. Meteorol. Soc. Jpn.*, *91*, 91–141.
Nakajima, K., Y. Yamada, Y. O. Takahashi, M. Ishiwatari, W. Ohfuchi, and H. Y.Y. (2013b), The variety of forced atmospheric structure in response to tropical SST anomaly found in ape results, *J. Meteorol. Soc. Jpn.*, *91*, 93–143.
Neale, R. B., and B. J. Hoskins (2000), A standard test for agcms including their physical parametrizations: I: The proposal, *Atmos. Sci. Lett.*, *1*(2), 101–107.

Neelin, J. D., and I. M. Held (1987), Modeling tropical convergence based on the moist static energy budget, *Mon. Weather Rev.*, *115*(1), 3–12.
Oueslati, B., and G. Bellon (2013a), Tropical precipitation regimes and mechanisms of regime transitions: Contrasting two aquaplanet general circulation models, *Clim. Dyn.*, *40*(9-10), 2345–2358.
Oueslati, B., and G. Bellon (2013b), Convective entrainment and large-scale organization of tropical precipitation: Sensitivity of the CNRM-CM5 hierarchy of models, *J. Clim.*, *26*(9), 2931–2946.
Peatman, S. C., A. J. Matthews, and D. P. Stevens (2014), Propagation of the Madden–Julian Oscillation through the maritime continent and scale interaction with the diurnal cycle of precipitation, *Q. J. R. Meteorol. Soc.*, *140*(680), 814–825.
Piriou, J.-M., J.-L. Redelsperger, J.-F. Geleyn, J.-P. Lafore, and F. Guichard (2007), An approach for convective parameterization with memory: Separating microphysics and transport in grid-scale equations, *J. Atmos. Sci.*, *64*(11), 4127–4139.
Raymond, D. J., S. L. Sessions, A. H. Sobel, and Ž. Fuchs (2009), The mechanics of gross moist stability, *J. Adv. Model. Earth Syst.*, *1*, 9, doi:10.3894/JAMES.2009.
Rio, C., F. Hourdin, F. Couvreux, and A. Jam (2010), Resolved versus parameterized boundary layer plumes. Part II: A continuous formulation of mixing rates for mass-flux schemes, *Boundary Layer Meteorol.*, *135*, 469–483, doi:10.1007/s10546-010-9478-z.
Roundy, P. E. (2012), The spectrum of convectively coupled kelvin waves and the madden-julian oscillation in regions of low-level easterly and westerly background flow, *J. Atmos. Sci.*, *69*(7), 2107–2111.
Semane, N., and P. Bechtold (2015), Convection and waves on small earth and deep atmosphere, *Tellus, Ser. A*, *67*, 25151, doi:http://dx.doi.org/10.3402/tellusa.v67.25151.
Sobel, A., and E. Maloney (2012), Moisture modes and the eastward propagation of the MJO, *J. Atmos. Sci.*, 187–192, doi:10.1175/JAS-D-12-0189.1.
Stevens, B., and S. Bony (2013), What are climate models missing, *Science*, *340*(6136), 1053–1054.
Swinbank, R., T. Palmer, and M. Davey (1988), Numerical simulations of the Madden and Julian Oscillation, *J. Atmos. Sci.*, *45*(5), 774–788.
Taylor, K., R. Stouffer, and G. Meehl (2012), An overview of CMIP5 and the experiment design, *Bull. Am. Meteorol. Soc.*, *93*, 485–498.
Tiedtke, M. (1989), A comprehensive mass flux scheme for cumulus parameterization in large-scale models, *Mon. Weather Rev.*, *117*(8), 1779–1800.
Voigt, A., and T. A. Shaw (2015), Circulation response to warming shaped by radiative changes of clouds and water vapour, *Nat. Geosci.*, *8*(2), 102–106.
Voldoire, A., et al. (2013), The CNRM-CM5.1 global climate model: Description and basic evaluation, *Clim. Dyn.*, *40*(9-10), 2091–2121.
Waliser, D. E., K. Lau, W. Stern, and C. Jones (2003), Potential Predictability of the Madden–Julian Oscillation., *Bull. Am. Meteorol. Soc.*, *84*(1), 33–50, doi:http://dx.doi.org/10.1175/BAMS-84-1-33.
Waliser, D. E., et al. (2009), MJO simulation diagnostics, *J. Clim.*, *22*(11), 3006–3030, doi:10.1175/2008JCLI2731.1.
Walters, D., et al. (2011), The Met Office Unified Model Global Atmosphere 3.0/3.1 and JULES Global Land 3.0/3.1 configurations, *Geosci. Model Dev. Discuss.*, *4*(2), 1213–1271.
Wang, B., P. Webster, K. Kikuchi, T. Yasunari, and Y. Qi (2006), Boreal summer quasi-monthly oscillation in the global tropics, *Clim. Dyn.*, *27*(7-8), 661–675.
Wheeler, M., and G. N. Kiladis (1999), Convectively coupled equatorial waves: Analysis of clouds and temperature in the wavenumber-frequency domain, *J. Atmos. Sci.*, *56*, 374–399.
Williamson, D. L., M. Blackburn, and K. Nakajima (2013), The aqua-planet experiment (ape): Response to changed meridional sst profile (special issue on the aqua-planet experiment project (ape) and related researches), *J. Meteorol. Soc. Jpn.*, *91*, 57–89.
Xavier, P. K., et al. (2015), Vertical structure and physical processes of the madden-julian oscillation: Biases and uncertainties at short range, *J. Geophys. Res. Atmos.*, *120*, 4749–4763, doi:10.1002/2014JD022718.
Zhang, C. (2005), Madden-Julian Oscillation, *Rev. Geophys.*, *43*, RG2003, doi:10.1029/2004RG000158.
Zhang, C., J. Gottschalck, E. D. Maloney, M. W. Moncrieff, F. Vitart, D. E. Waliser, B. Wang, and M. C. Wheeler (2013), Cracking the MJO nut, *Geophys. Res. Lett.*, *40*, 1223–1230, doi:10.1002/grl.50244.